# Class IIa HDACs reprogram mitochondrial metabolism to inhibit apoptosis and ferroptosis in response to lipotoxicity

Sheree D. Martin[1,9], Timothy Connor[1,9], Andrew Sanigorski[1], Kevin A. McEwen[1], Darren C. Henstridge[2,3], Brunda Nijagal[4], David De Souza[4], Dedreia L. Tull[4], Peter J. Meikle[3], Greg M. Kowalski[1,5], Clinton R. Bruce[5], Paul Gregorevic[6], Mark A. Febbraio[7], Fiona M. Collier[8], Ken R. Walder[1], Sean L. McGee[1,10]

[1]Institute for Mental and Physical Heath and Clinical Translation (IMPACT) and Metabolic Research Unit, School of Medicine, Deakin University, Geelong, Victoria 3216, Australia;
[2]College of Health and Medicine, School of Health Sciences, University of Tasmania, Launceston, Australia;
[3]Baker Heart and Diabetes Institute, Melbourne, Victoria 3004, Australia;
[4]Metabolomics Australia, The University of Melbourne, Parkville, Victoria 3010, Australia;
[5]Institute of Physical Activity and Nutrition (IPAN) and School of Exercise and Nutrition Sciences, Deakin University, Geelong, Victoria 3216, Australia;
[6]Centre for Muscle Research, Department of Anatomy and Physiology, The University of Melbourne, Parkville, VIC, Australia.
[7]Monash Institute of Pharmaceutical Sciences, Monash University, Parkville, VIC, Australia.
[8]Barwon Health, Geelong, Victoria 3220, Australia
[9]These authors contributed equally to this work
[10]Lead contact

Lead contact:

Professor Sean L. McGee
Metabolic Remodelling Laboratory
Metabolic Research Unit
School of Medicine
Deakin University, Waurn Ponds, Australia, 3216
Ph: +61 3 5227 2519
Fax: +61 3 5227 2945
Email: sean.mcgee@deakin.edu.au

**ABSTRACT**

Lipotoxicity, the accumulation of lipids in non-adipose tissues, alters the metabolic transcriptome and mitochondrial metabolism in skeletal muscle. The mechanisms involved remain poorly understood. Here we show that lipotoxicity increased histone deacetylase 4 (HDAC4) and histone deacetylase 5 (HDAC5), which reduced the expression of metabolic genes and oxidative metabolism in skeletal muscle. This metabolic reprogramming was linked with reduced expression of p53-dependent genes that mediate apoptosis and ferroptosis, which preserved cell viability in response to lipotoxicity. Mechanistically, impaired mitochondrial metabolism reduced acetylation of p53 at K120, a modification required for transcriptional activation of apoptosis, while redox drivers of ferroptosis were also reduced. Overexpression of loss-of-function HDAC4 and HDAC5 mutants in skeletal muscle of obese *db/db* mice enhanced oxidative capacity, increased apoptosis and ferroptosis and reduced muscle mass. This study identifies HDAC4 and HDAC5 as repressors of the oxidative state of skeletal muscle, and that this metabolic reprogramming, considered deleterious for normal metabolism, is critical to preserve muscle integrity in response to lipotoxicity.

## INTRODUCTION

Obesity is driving an epidemic of chronic disease, including type 2 diabetes, non-alcoholic fatty liver disease, cardiovascular disease and cancer. Linked to many of these diseases are adverse cellular responses arising from the accumulation of lipids in non-adipose tissues, a process that has been termed lipotoxicity[1]. The deleterious effects of lipotoxicity, which include altered cellular signalling, metabolic reprogramming and apoptotic cell death[2], are thought to be mediated by bioactive lipid species such as diglycerides (DG) and ceramides[3]. In contrast, the accumulation of neutral lipids such as triglycerides (TG) is thought to protect against the harmful effects of lipotoxicity[4]. Tissues that are particularly susceptible to lipotoxicity include the liver, kidneys, pancreas, heart and skeletal muscle[2].

Alterations in skeletal muscle metabolism occur in obesity, including insulin resistance and impairments in several aspects of oxidative metabolism. Reduced rates of both glucose and lipid oxidation have been observed in the skeletal muscle of obese patients[5, 6] and data describing alterations in amino acid metabolism are also emerging[7, 8, 9]. While methodological caveats to some of these studies have been raised[10], these impairments in oxidative metabolism are associated with reduced expression of a metabolic and mitochondrial transcriptional program controlled by the peroxisome proliferator-activated receptor-gamma coactivator 1 alpha (PGC-1$\alpha$) transcriptional coactivator[11], encoded by the *PPARGC1A gene*. Furthermore, down-regulation of this PGC-1$\alpha$-dependent transcriptional program is also associated with insulin resistance[12], although studies using several animal models have questioned the relationship between PGC-1$\alpha$ and skeletal muscle insulin action[13, 14].

Experimental induction of acute lipotoxicity in humans through lipid infusion results in many of the same skeletal muscle metabolic alterations that are observed in obesity. These include insulin resistance, reduced substrate oxidation and impairment of mitochondrial function[15], as well as reduced expression of *PPARGC1A* and genes involved in mitochondrial and metabolic processes[16]. Moreover, transcriptional reprogramming of metabolism, like that in obesity, is observed when muscle cells are cultured with elevated concentrations of the saturated fatty acid palmitate[17, 18, 19]. It is not known why repression of the metabolic transcriptome and reduced oxidative metabolism is an adaptation to lipotoxicity and the molecular pathways involved remain unclear. Furthermore, how these metabolic adaptations influence other responses to lipotoxicity, such as cell signalling and cell death responses, are unknown.

Studies from our group and others have found that the class IIa histone deacetylase (HDAC) isoforms 4 and 5 are regulators of PGC-1$\alpha$ expression and oxidative metabolism in skeletal muscle[20, 21]. HDAC4 and 5 act co-operatively as heterodimers to repress the myocyte-enhancer factor 2 (MEF2) family of transcription factors[22, 23]. The ability of the class IIa HDACs to repress MEF2 transcriptional activity is prevented by phosphorylation-dependent nuclear export[24]. HDAC4 and 5 are also sensitive to energetic stress, such as during exercise, through phosphorylation by the AMP-activated protein kinase (AMPK)[25, 26, 27], which in turn activates transcriptional programs that enhance oxidative metabolism and capacity, including expression of PGC-1$\alpha$ and its transcriptional programs[20, 27, 28]. Binding sites for the MEF2 transcription factor are found in the *PPARGC1A* promoter[21] and in the promoters and

107 enhancer regions of other genes involved in oxidative metabolism[20]. Together, these
108 findings suggest that the class IIa HDACs are a critical hub regulating skeletal muscle
109 metabolic transcriptional programs in response to changes in energy balance. However, the
110 role of the class IIa HDAC transcriptional repressors in regulating metabolic transcriptional
111 programs and oxidative metabolism in the context of lipotoxicity is unknown. The current
112 study sought to determine whether HDAC4 and 5 contribute to the suppression of
113 metabolic genes and oxidative metabolism in response to lipotoxicity and to explain why
114 these adaptations occur.

## RESULTS

### HDAC4 and 5 are increased in models of lipotoxicity

To test the hypothesis that HDAC4 and 5 are increased by lipotoxicity, cultures of C2C12 myotubes were exposed to 0.25 or 0.5mM palmitate, or BSA (vehicle), for 16 hr. Exposure to both 0.25 and 0.5mM palmitate did not negatively impact cell viability, assessed by lactate dehydrogenase (LDH) release (Supplementary Fig. 1A). Lipidomic profiling indicated ceramide and DG species were increased following exposure to 0.5mM palmitate, while increases in some TG species were observed following exposure to both 0.25mM and 0.5mM palmitate (Figure 1A). Total Cer levels were increased by both 0.25mM and 0.5mM palmitate while total DG and TG levels were increased by 0.5mM palmitate (Figure 1B). Consistent with the known effect of palmitate on C2C12 cells, application of 0.5mM palmitate was associated with a non-significant trend for *Ppargc1a* gene expression to be reduced (Fig. 1C) and a significant reduction in cellular respiration (Fig. 1D). The abundance of HDAC5 protein was increased by both 0.25 and 0.5mM palmitate, while HDAC4 protein abundance was increased by 0.5mM palmitate (Figure 1E). There were no differences in *Hdac4* gene expression between groups, while *Hdac5* gene expression was reduced by 0.5mM palmitate (Supplementary Fig. 1B).

To examine these mechanisms *in* vivo, the tibialis anterior skeletal muscle of obese *db/db* and control heterozygous littermate mice was analysed. Specific ceramide, DG and TG species (Fig. 1F) and total ceramides and DG were increased in skeletal muscle of *db/db* mice (Fig. 1G). The increased muscles lipid concentrations in these obese mice were associated with decreased *Ppargc-1*$\alpha$ gene expression (Fig. 1H), reduced respiratory responses in skeletal muscle biopsies (Fig. 1I) and increased HDAC4 and 5 protein abundance (Fig. 1J). Skeletal muscle gene expression levels of *Hdac5*, but not *Hdac4*, were increased in *db/db* mice (Supplementary Fig. 1C). Together, these data suggest that skeletal muscle HDAC4 and 5 are increased in response to lipotoxicity and are associated with reduced *Ppargc1a* expression and impaired oxidative metabolism.

### Overexpression of HDAC4 and 5 in skeletal muscle represses *Pppargc1a* expression and oxidative capacity

To determine whether increased HDAC4 and 5 reduces *Ppargc1a* gene expression and impairs oxidative capacity in skeletal muscle, a bilateral skeletal muscle HDAC4 and 5 mouse model was developed using recombinant serotype 6 adeno-associated viral (AAV6) vectors expressing HDAC4 and HDAC5 (Fig. 2A). Administration of HDAC4 and 5 AAV6 vectors increased *Hdac4* and *Hdac5* gene expression (Fig. 2B) and HDAC4 and 5 protein (Fig. 2C) in tibialis anterior muscle. Overexpression of HDAC4 and 5 reduced *Ppargc1a* expression (Fig. 2D). Furthermore, HDAC4 and 5 overexpression reduced the expression of a range of MEF2 and PGC-1$\alpha$ target genes involved in oxidative and mitochondrial metabolism (Fig. 2E). These changes in metabolic transcripts were associated with reduced abundance of ATP synthase subunits, but not other subunits of electron transport chain complexes (Fig. 2F). To establish whether reduced ATP synthase components resulted in reduced oxidative capacity, respiration was assessed in skeletal muscle biopsies. There were overall main effects for respiratory responses to be reduced in muscles overexpressing HDAC4 and 5

when driven by both succinate (Fig. 2G) and malate (Fig. 2H) as substrates. The reduction in oxidative capacity in skeletal muscle overexpressing HDAC4 and 5 was not associated with the accumulation of any lipid species examined, although all lipid species tended to be higher in skeletal muscle overexpressing HDAC4 and 5 (Fig. 2I). These data indicate that increasing HDAC4 and 5 represses *Ppargc1a* gene expression and oxidative metabolism in skeletal muscle.

The class IIa HDACs form heterodimers, which influences their repressive functions and sensitivity to upstream signalling pathways[22]. To investigate the separate role of HDAC4 and 5 in repression of *Ppargc1a* gene expression, HDAC4 and 5 were individually overexpressed in skeletal muscle with increasing doses of AAV6 vectors (Supplementary Fig. 2A). Treatment of muscles with AAV vectors expressing HDAC4 or HDAC5 resulted in dose dependent increases in the expression of *Hdac4* and *Hdac5* genes (Supplementary Fig. 2B) and increased HDAC4 and 5 protein abundance (Supplementary Fig. 2C). Overexpression of HDAC4 at both AAV6 doses reduced *Ppargc1a* gene expression (Supplementary Fig. 2D). Similarly, overexpression of HDAC5 using both AAV doses was sufficient to reduce *Ppargc1a* expression (Supplementary Fig. 2E). Together, these data suggest that increases in either HDAC4 or HDAC5 can repress *Ppargc1a* gene expression.

**Overexpression of HDAC4 and 5 in skeletal muscle inhibits oxidative glucose utilisation**

Impaired skeletal muscle oxidative metabolism and mitochondrial function associated with lipotoxicity have been linked with reduced insulin action and impaired glucose utilisation[6, 12, 29]. As HDAC4 and 5 overexpression reduced skeletal muscle oxidative capacity, the impact of HDAC4 and 5 overexpression on glucose metabolism was examined. Bilateral skeletal muscle HDAC4 and 5 mice were administered vehicle or insulin (1.2U/kg i.p.) with $^{3}$H-2-deoxyglucose (2-DG) and $^{14}$C-glucose tracers 30 min prior to tissues collection (Fig. 3A). Insulin reduced the excursion of both tracers (Supplementary Fig. 3A and B). There was a main effect for increased glucose clearance by skeletal muscles overexpressing HDAC4 and 5 (Fig. 3B). When expressed relative to control skeletal muscle within each mouse, muscles with HDAC4 and 5 overexpression increased glucose clearance in vehicle but not insulin-stimulated conditions (Figure 3C). Overexpression of HDAC4 and 5 increased glucose incorporation into glycogen (Fig. 3D) and increased glycogen concentration (Supplementary Fig. 3C). In contrast there was a main effect for insulin to increase glucose incorporation into lipids (Fig. 3E), which was associated with main effects for insulin to increase Akt phosphorylation at both of its main regulatory sites at T308 (Fig. 3G) and S473 (Fig. 3H). However, consistent with the glucose clearance data, there was a main effect for increased phosphorylation of TBC1D4 at S642 in skeletal muscles overexpressing HDAC4 and 5 (Fig. 3I). These data suggest that overexpression of HDAC4 and 5 increased non-oxidative glucose utilisation in skeletal muscle.

To further examine the effect of HDAC4 and 5 overexpression on oxidative glucose utilisation, a targeted stable isotope metabolomics approach following an oral bolus of U$^{13}$C-glucose was used in bilateral skeletal muscle HDAC4 and 5 mice[30] (Fig. 3J). Overexpression of HDAC4 and 5 increased the abundance of lactate and succinate (Fig. 3K) and total $^{13}$C labelling of succinate and malate (Fig. 3L). Isotopologue analysis revealed accumulation of both M+0 and M+2 lactate in muscle overexpressing HDAC4 and 5 (Fig.

3M), suggesting both increased non-oxidative glucose utilisation and increased malate/pyruvate cycle flux, respectively[31]. Succinate M+0, M+1 and M+2 isotopologues were increased in muscle overexpressing HDAC4 and 5 (Fig. 3N), consistent with a major impairment in SDH activity[32], which is bifunctional for both the TCA cycle and the electron transport chain. These data are also supported by reduced succinate-driven respiration in muscles overexpressing HDAC4 and 5 (Fig. 2G). Similarly, HDAC4 and 5 overexpression was associated with increased malate M+0 and M+1 isotopologues (Fig. 3O). Together, these data indicate that increased HDAC4 and 5 is linked with defective oxidative utilisation of glucose in skeletal muscle.

**HDAC4 and 5 enhance cell survival in response to lipotoxicity and supress the apoptosis and ferroptosis cell death pathways**

Overexpression of HDAC4 and 5 impaired mitochondrial function and reprogrammed glucose metabolism, increasing non-oxidative glucose utilisation and inhibiting oxidative glucose utilisation. In doing so, increased HDAC4 and 5 replicate some, but not all, of the metabolic alterations seen during lipotoxicity. To better understand why this metabolic reprogramming occurs, a comparative transcriptomics approach was employed. Specifically, the transcriptome altered in the skeletal muscle of *db/db* mice in which HDAC4 and 5 was increased (Fig. 1J) was compared to the transcriptome altered in C2C12 myoblasts stably overexpressing HDAC4 and 5 (Supplementary Fig. 4A). These cultured C2C12 cells were used to increase the biological diversity in this comparison and were analysed as myoblasts, as HDAC4 and 5 overexpression prevented their differentiation into myotubes (data not shown). Nonetheless, HDAC4 and 5 overexpression in C2C12 myoblasts induced phenotypic characteristics consistent with HDAC4 and 5 overexpression in skeletal muscle, including reduced *Ppargc1a* gene expression, suppression of a broad metabolic transcriptional program, including reduced OXPHOS and TCA cycle pathways, and reduced oxidative capacity (Supplementary Fig. 4B-D). Comparison of the transcriptome altered in the skeletal muscle of *db/db* mice to that altered in C2C12 myoblasts overexpressing HDAC4 and 5 and subsequent pathway analysis of coregulated genes revealed the p53 signalling pathway as the only significantly regulated pathway (Supplementary Fig. 4E).

Profiling of p53-dependent genes in C2C12 myoblasts overexpressing HDAC4 and 5 revealed that several pro-apoptosis genes were reduced, including *Casp9, Cycs, Pmaip1* and *Bbc3* (Fig. 4A), consistent with suppression of apoptosis. Similarly, genes involved in ferroptosis, which is a form of iron-mediated cell death involving lipid peroxidation[33], were altered in a way that indicated suppression of ferroptosis, via increased *Slc7a11* expression and reduced *Sat1* and *Alox15* expression (Fig. 4A). Together, these data suggest that increased HDAC4 and 5 inhibit apoptotic and ferroptotic cell death pathways. To test this hypothesis, C2C12 myoblasts overexpressing HDAC4 and 5 were treated with agents that induce either apoptosis or ferroptosis. Overexpression of HDAC4 and 5 in C2C12 myoblasts reduced the number of early apoptotic cells (Annexin$^{+}$/PI$^{-}$) following exposure to the apoptosis-inducing agent camptothecin (Fig. 4B). Similarly, overexpression of HDAC4 and 5 increased the percentage of viable cells following exposure to the ferroptosis-inducing agent RSL3 (Fig. 4C). These data raised the possibility that HDAC4 and 5 suppress the apoptosis and ferroptosis pathways to enhance cell survival in response to lipotoxicity. To test this hypothesis, cells were exposed to high concentrations of palmitate that were intended to

256 induce cytotoxicity. Overexpression of HDAC4 and 5 increased the viability of cells exposed
257 to both 1 and 2mM of palmitate compared with control cells and resulted in cells being
258 largely resistant to lipotoxicity (Fig. 4D). This protection of cell viability in response to
259 lipotoxicity was associated with reduced cleavage of caspase 3 and 9, the irreversible events
260 that trigger apoptosis (Fig. 4E), as well as fewer cells in both early (Fig. 4F) and late (Fig. 4G)
261 apoptosis in response to increasing concentrations of palmitate. Similarly, overexpression of
262 HDAC4 and 5 reduced lipid peroxidation, the trigger for ferroptosis induced-cell death, in
263 response to increasing concentrations of palmitate (Fig. 4H). These data indicate that
264 increased HDAC4 and 5 inhibit the apoptosis and ferroptosis cell death pathways and
265 enhance cell survival in response to lipotoxicity.
266
267 **HDAC4 and 5 inhibit apoptosis by reducing p53 K120 acetylation, which is regulated by**
268 **HDAC4 and 5-mediated alterations in metabolism**
269
270 In several cancer cell types, increased HDAC5 has been linked with reduced acetylation of
271 p53 at K120, which inhibits p53 DNA binding and the expression of p53-dependent
272 apoptosis genes, and reduces apoptosis sensitivity[34, 35, 36]. Furthermore, acetylation of p53,
273 including at K120, is linked to the transcriptional regulation of ferroptosis[37]. To explore
274 whether reduced acetylation of p53 at K120 by HDAC4 and 5 is involved in suppression of
275 apoptosis and ferroptosis in myogenic cells, C2C12 myoblasts stably overexpressing HDAC4
276 and 5 were transfected with wild type p53, or p53 in which K120 was mutated to either
277 glutamine (K120Q; acetylation mimetic gain-of function) or arginine (K120R; deacetylation
278 mimetic loss-of-function) (Fig. 5A). The acetylation of p53 at K120 was reduced by the
279 overexpression of HDAC4 and 5 (Fig. 5A). In cells overexpressing HDAC4 and 5, introduction
280 of the $p53^{K120Q}$ acetylation mimetic mutant restored the expression of the pro-apoptosis
281 genes *Casp3, Casp9* and *Cycs* (Fig. 5B). However, the expression of *Slc7a11*, which opposes
282 ferroptosis, was not influenced by expression of this mutant (Fig. 5B). This suggests that
283 reduced acetylation of p53 at K120 by increased HDAC4 and 5 is involved in the
284 transcriptional suppression of apoptosis, but not ferroptosis cell death pathways. Indeed,
285 expression of $p53^{K120Q}$ also restored apoptosis in HDAC4 and 5 overexpressing cells exposed
286 to the apoptosis-inducing agent camptothecin (Fig. 5C). Although p53 is also known to
287 regulate aspects of cellular metabolism[38], gain and loss-of-function K120 mutants had no
288 effect on either oxidative (Supplementary Fig. 5A) or glycolytic flux (Supplementary Fig. 5B).
289 These data show that reduced acetylation of p53 at K120 contributes to inhibition of
290 apoptosis by HDAC4 and 5 in myogenic cells.
291
292 The class IIa HDACs have a unique amino acid substitution within their HDAC active site that
293 confers low deacetylase activity against acetyl-lysine[39], indicating that it is unlikely that
294 HDAC4 or 5 are direct p53 deacetylases. We explored the possibility that K120 p53
295 acetylation is sensitive to the HDAC4 and 5-mediated reduction in oxidative metabolic flux
296 that reduces acetyl-CoA availability for acetylation reactions. To test this hypothesis,
297 substrate tracer incorporation into K120 of p53 was examined. Exposure of control cells to
298 $^{14}$C-palmitate resulted in isotope incorporation into wild type (WT) p53, with only limited
299 isotope incorporation into mutant $p53^{K120R}$ (Fig. 5D). There was significantly lower tracer
300 incorporation into both WT and $p53^{K120R}$ in cells overexpressing HDAC4 and 5 (Fig. 5D).
301 There was negligible tracer incorporation into p53 when cells were exposed to $^{14}$C-glucose

302 (Fig. 5D). This suggests that carbon derived from fatty acids but not glucose is used for
303 apoptosis-inducing post-translational modification of p53 at K120.
304
305 The acetyl-CoA required for cytosolic and nuclear acetylation reactions is derived from
306 citrate that is exported from the TCA cycle by the mitochondrial citrate transporter[40]. Once
307 exported from the mitochondria, citrate is converted to acetyl-CoA by ATP-citrate lyase,
308 whose activity is increased by insulin[41]. To determine whether HDAC4 and 5 control p53
309 K120 acetylation via mitochondrial metabolism, cells were treated with vehicle or insulin in
310 the presence or absence of the citrate transport inhibitor, 1,2,3-benzenetricarboxylate
311 (BTC). In the non-mitochondrial fraction of control cells, insulin increased acetylation of p53
312 at K120, which was reduced by exposure to BTC (Fig. 5E). However, acetylation of p53 at
313 K120 was completely abrogated in cells overexpressing HDAC4 and 5. These findings show
314 that K120 acetylation is dependent on mitochondrial metabolism and acetyl-CoA
315 availability. Consistent with a requirement for acetyl-CoA in p53 K120 acetylation, acetyl-
316 CoA levels were reduced in cells overexpressing HDAC4 and 5 (Fig. 5F).
317
318 To determine whether p53 K120 acetylation determines cell viability in response to
319 lipotoxicity, cells expressing WT p53 or $p53^{K120R}$ were exposed to 2mM palmitate. However,
320 the $p53^{K120R}$ mutant did not influence cell viability at any time point after palmitate
321 exposure (Fig. 5G), suggesting that other mechanisms are also involved in the cell death
322 response to lipotoxicity. Nonetheless, these data show that HDAC4 and 5 inhibit apoptosis
323 by reducing the acetylation of p53 at K120, which is sensitive to HDAC4 and 5-mediated
324 alterations in mitochondrial metabolism. However, this inhibition of p53 K120 acetylation
325 alone is not sufficient to prevent cell death in response to lipotoxicity.
326
327 **HDAC4 and 5 regulate multiple metabolic inputs to the ferroptosis pathway**
328
329 As suppression of apoptosis through reduced p53 acetylation alone was not sufficient to
330 explain the protective effect of HDAC4 and 5 on cell survival in response to lipotoxicity, the
331 role of ferroptosis-mediated mechanisms of cell death (Fig. 6A) were further explored. The
332 ferroptosis inhibitor Ferrostatin enhanced C2C12 myoblast viability following exposure to
333 2mM palmitate (Fig. 6B), suggesting that ferroptosis contributes to lipotoxicity-mediated
334 cell death. Overexpression of HDAC4 and 5 enhanced cell viability in response to increasing
335 concentrations of Erastin (Fig. 6C), an agent that induces ferroptosis by inhibiting system $x_c$
336 and glutamate and cysteine exchange[42], which in turn reduces glutathione (GSH) levels and
337 results in lipid peroxidation through multiple mechanisms (Fig. 6A). Consistent with HDAC4
338 and 5 increasing the expression of *Slc7a11* (Fig. 4A), overexpression of HDAC4 and 5
339 reduced intracellular glutamate concentrations, tended to increase intracellular GSH and
340 increased the GSH/glutamate ratio (Fig. 6D). This was associated with increased glutathione
341 peroxidase (GPX) activity in cells overexpressing HDAC4 and 5 (Fig. 6E) and reduced total
342 $H_2O_2$ production (Supplementary Fig. 6A), including from mitochondria and NADPH oxidases
343 (Fig. 6F). Together, these data indicate that increased HDAC4 and 5 alters the metabolism-
344 sensitive redox inputs to ferroptosis consistent with inhibition of this pathway.
345
346 Ferroptosis involves peroxidation of polyunsaturated (PU) phosphatidylethanolamine (PE)
347 and phosphatidylcholine (PC) lipids, particularly those with arachidonic acid (AA) or adrenic
348 acid (Ada) fatty acid species[43]. Changes in the levels of these lipid species have been linked

349 to alterations in ferroptosis sensitivity[43]. In lipidomic data from skeletal muscle bilateral
350 HDAC4 and 5 mice, overexpression of HDAC4 and 5 had no effect on any specific PU-PE or
351 PU-PC species between groups, although most lipid species tended to be higher in muscle
352 overexpressing HDAC4 and 5 (Supplementary Fig. 6B). However, it should be noted that
353 HDAC4 and 5 reduced the gene expression of *Alox15* (Fig. 4A), which catalyses lipid
354 peroxidation (Fig. 6A), and of *Sat1* (Figure 4A), which is a transcriptional regulator of *Alox15*
355 and a p53 target gene[44]. The extent of lipid saturation has also been linked to lipotoxicity
356 induced cell death[45], however there were no differences in lipid saturation when expressed
357 either as absolute abundance (Supplementary Fig. 6C) or proportion of total lipids
358 (Supplementary Fig. 6D). This suggests that HDAC4 and 5 have minimal effect on the
359 abundance of lipid species but reduces expression of enzymes that mediate lipid
360 peroxidation. Together, these findings indicate that increased HDAC4 and 5 alter cellular
361 redox balance and expression of *Alox15*, which contributes to inhibition of ferroptosis.
362
363 **HDAC4 and 5 are required to suppress apoptosis and ferroptosis and maintain muscle**
364 **mass in obese mice**
365
366 To establish whether HDAC4 and 5 suppress apoptosis and ferroptosis in skeletal muscle in
367 response to lipoxicity *in vivo*, a bilateral skeletal muscle loss-of-function HDAC4 and 5 model
368 was developed in obese *db/db* mice using AAV6 vectors (Fig. 7A). This loss-of-function
369 approach employed active-site HDAC4 and 5 mutants (D832N HDAC4 and D861N HDAC5),
370 which we have previously described as acting in a dominant negative (DN) manner when
371 overexpressed[20]. Overexpression of these mutants in skeletal muscle increases the
372 expression of *Ppargc1a* and other metabolic genes and enhance oxidative metabolism[20].
373 Intramuscular administration of AAV6 vectors expressing DN HDAC4 and 5 to *db/db* mice
374 increased HDAC4 and 5 gene (Fig. 7B) and protein (Fig. 7C) expression and increased the
375 expression of *Ppargc1a* (Fig. 7D). Consistent with these findings, there was a main effect for
376 respiratory responses to be increased in muscle biopsies expressing DN HDAC4 and 5 (Fig.
377 7E). Expression of DN HDAC4 and 5 modestly increased caspase 3 activity (Fig. 7F) and lipid
378 peroxidation (Fig. 7G), functional readouts of apoptosis and ferroptosis, respectively.
379 Examination of the mechanisms involved in HDAC4 and 5-mediated apoptosis revealed that
380 p53 acetylation of K120 tended to be higher (Fig. 7H), and the expression of p53-dependent
381 pro-apoptosis genes, including *Casp3, Casp9* and *Bbc3* was increased (Fig. 7I). The
382 ferroptosis mechanisms regulated by HDAC4 and 5 were also examined. In contrast to
383 observations in myogenic cells, the expression of *Slc7a11* in skeletal muscle was low and
384 close to assay detection limits (Supplementary Fig. 7A). This suggests that system $x_c$ has only
385 a minor role in the regulation of ferroptosis in skeletal muscle. There were no differences in
386 GPX activity between groups (Supplementary Fig. 7B). However, expression of DN HDAC4
387 and 5 increased ROS (Fig. 7J) and increased *Sat1* and *Alox15* expression (Fig. 7K), indicating
388 that increased capacity for lipid peroxidation. Increased apoptosis and ferroptosis in skeletal
389 muscles expressing DN HDAC4 and 5 was associated with reduced mass of the
390 gastrocnemius and the TA muscles (Fig. 7L). In the TA muscle, there was no difference in
391 fibre diameter between groups (Supplementary Fig. 7C). However, Masson's trichrome
392 staining showed sporadic areas of localised fibrosis in response to DN HDAC4 and 5
393 overexpression (Fig. 7M). In skeletal muscles overexpressing DN HDAC4 and 5 there were
394 also discreet regions of fibres with centralised nuclei (Fig. 7N), which is indicative of

395 regenerating muscle fibres. These data show that HDAC4 and 5 are required to suppress
396 apoptosis and ferroptosis and to maintain muscle mass in skeletal muscle of obese mice.

397 **DISCUSSION**
398
399 Lipotoxicity has a major impact on the metabolism, function and survival of various tissues
400 including skeletal muscle. The current study has revealed that increases in HDAC4 and 5 in
401 response to lipotoxicity induce transcriptional repression of oxidative metabolism and of the
402 apoptosis and ferroptosis cell death pathways in both myogenic cells and skeletal muscle
403 (Fig. 8A and B). The impairment in oxidative metabolism is directly linked to reduced p53
404 acetylation at K120 and inhibition of a pro-apoptosis transcriptional program. Furthermore,
405 metabolic reprogramming to a lower oxidative state also impacted multiple redox inputs to
406 ferroptosis, which inhibited this pathway. These data indicate that metabolic
407 reprogramming in skeletal muscle in response to lipotoxicity is directly linked with cell
408 survival responses.
409
410 Previous findings revealed that lipotoxicity is associated with suppression of a pro-apoptosis
411 transcriptional program in skeletal muscle, with consequences for maintenance of muscle
412 mass[46]. Our data show that the class IIa HDACs are essential for this response, as loss of
413 HDAC4 and 5 function in skeletal muscle in a model of lipotoxicity increased apoptosis genes
414 and markers of apoptosis, which was associated with reduced muscle mass. Furthermore, a
415 readout of ferroptosis was also increased. The exact contribution of these cell death
416 pathways to the reduction in muscle mass observed remains to be determined. However,
417 identification that p53 acetylation at K120 is sensitive to substrate supply, metabolic flux
418 and acetyl-CoA availability is an important finding linking metabolism to cell survival
419 responses and has implications for several metabolic diseases, including cancer. As acetyl-
420 CoA operates at the crossroads of catabolic and anabolic metabolism, it seems rational to
421 hypothesise that this metabolite is involved in linking metabolic sensing to cell signalling and
422 adaptive responses. These findings also provide insights into why some substrates are more
423 cytotoxic than others when in excess. It is well established that saturated fatty acids, such as
424 palmitate, are more effective at inducing cell death than unsaturated fatty acids such as
425 oleate[4]. Palmitate is more readily oxidised than oleate[4], thus increasing the acetyl-CoA pool,
426 which would place pressure on K120 p53 acetylation and apoptosis responses. This concept
427 was supported by our tracer data showing much lower overall carbon enrichment into p53
428 from glucose when compared with that derived from palmitate. Indeed, there are many
429 fates for the carbon derived from glucose in comparison to that derived from fatty acids,
430 which must form mitochondrial acetyl-CoA as a process of β-oxidation.
431
432 While there is much debate in the literature about the relationship between mitochondrial
433 capacity and function and insulin action[10], the reduction in oxidative capacity induced by
434 HDAC4 and 5 did not result in overt insulin resistance. Overexpression of HDAC4 and 5
435 increased basal glucose clearance, with more glucose directed to glycogen synthesis.
436 Oxidative utilisation of glucose was impaired through the TCA cycle, particularly at the level
437 of succinate, which was consistent with decreased succinate-driven respiration. The levels
438 of succinate are thought to reflect the redox state of the mitochondrial coenzyme Q pool,
439 with increased reduced CoQ ($CoQH_2$) preventing the oxidation of succinate by SDH[47].
440 Impairments in electron transport chain complexes, such as that observed in the current
441 study, are therefore linked to inhibition of succinate oxidation[48]. Furthermore, oxidation of
442 succinate by SDH is tightly associated with reverse electron flow to complex I of the electron
443 transport chain and ROS production[49]. Indeed, succinate oxidation-dependent ROS

444 production is critical for pro-inflammatory cytokine production by macrophages[50], adipose
445 tissue thermogenesis[51] and the activity of carotid body oxygen sensing $K^+$ channels[52]. In the
446 context of the present study, HDAC4 and 5-mediated impairments in succinate oxidation
447 and ROS production likely contribute to inhibition of the ferroptosis pathway and
448 preservation of cell viability in response to lipotoxicity. Additionally, impairments in TCA
449 cycle activity have recently been found to promote cytosolic glutathione synthesis that
450 increases antioxidant capacity[32], which would also inhibit ferroptosis. Together, these data
451 indicate that inhibition of oxidative substrate utilisation is an important adaptation to
452 lipotoxicity.
453
454 In conclusion, this study provides evidence that the class IIa HDACs link impairments in
455 skeletal muscle oxidative metabolism in response to lipotoxicity with inhibition of the
456 apoptosis and ferroptosis cell death pathways to preserve cell viability. This study has
457 identified new metabolic inputs to transcriptional control of the apoptosis pathway and
458 show that decreasing the overall oxidative state of skeletal muscle is also important for
459 inhibition of ferroptosis. These findings provide key new insights into why certain metabolic
460 adaptations occur in response to excess lipids and advance our understanding of the
461 aetiology of metabolic diseases driven by lipotoxicity and excess nutrient availability.

462 **MATERIALS AND METHODS**
463
464 **Plasmids and adeno-associated viral vectors**
465 cDNAs for mouse wild type HDAC4 and 5 were subcloned into pAAV-CMV-M and were
466 packaged into serotype 6 adeno-associated viruses (AAV), purified and titred as previously
467 described [53]. AAV6 vectors expressing DN HDAC4 and 5 have been previously described [20].
468 cDNAs for human wild type HDAC4 and HDAC5 were subcloned into pIRESneo3 and
469 pIREShyg3 vectors, respectively, to facilitate generation of stable cell lines. pcDNA3 Flag p53
470 (wild-type, human) was purchased from Addgene (plasmid #10838). Mutant p53 plasmids
471 (K120R and K120Q) were generated using the QuikChange XL Site-Directed Mutagenesis Kit
472 (Agilent Technologies).
473
474 **Cell culture**
475 Mouse C2C12 myoblasts (ATCC) expressing pIRES neo3 HDAC4 (wild-type, human) and pIRES
476 hyg3 HDAC5 (wild-type, human) were produced by transfection of plasmids with
477 Lipofectamine LTX and PLUS reagent (Life Technologies) following manufacturer's
478 instructions. Control cells were generated by transfection with empty plasmids. Stable
479 expression was achieved by multiple rounds of antibiotic selection (500ug/mL Hygromycin B
480 and 500ug/mL Geneticin; Invitrogen). Cells were maintained in growth media consisting of
481 MEM alpha (1g/L glucose; Invitrogen), 10% foetal bovine serum (FBS; In Vitro Technologies)
482 and antibiotic-antimycotic (100units/mL penicillin, 100µg/mL streptomycin and 0.25µg/mL
483 Amphotericin B; Life Technologies), with the addition of selection antibiotics, at 37°C in 10%
484 $CO_2$. For insulin-stimulated experiments, cells were treated for 15min with 0nM or 10nM
485 insulin (Humulin R; Eli Lilly) prior to protein collection. Treatment doses of palmitate (Sigma-
486 Aldrich), camptothecin (Sigma), Erastin (Sigma), 1S,3R-RSL 3 (Sigma), Ferrostatin
487 (Selleckchem) and 1,2,3-benzenetricarboxylate (BTC; Sigma) are reported in Figure legends
488 and were applied for 24h unless otherwise stated. Palmitate was dissolved in ethanol at
489 70$^{o}$C and diluted in ultrapure $H_2O$ before being conjugated to fatty acid-free BSA at 1:10
490 ratio (w/v). An ethanol and BSA solution without palmitate was prepared at the same time
491 for use as a vehicle. Both palmitate and vehicle solutions were aliquoted and stored at -
492 20$^{o}$C. Each cell culture experiment was performed at least twice.
493
494 **Animal models**
495 All animal experimentation was approved by the Deakin University Animal Ethics Committee
496 (G27-2012 and G21-2015), which is subject to the Australian Code for the Responsible
497 Conduct of Research. Mice were acquired from the Animal Resources Centre (Perth, WA,
498 Australia) and were group housed with a 12hr light/dark cycle, temperature 21± 3°C,
499 humidity: 30-70%. Animals had *ad libitum* access to standard rodent chow and water.
500 Heterozygous *db/+* and homozygous *db/db* mice were fasted for 5 hr prior to humane killing
501 by cervical dislocation for rapid excision of tissues, which were snap frozen in liquid nitrogen
502 for later analysis. C57Bl/6J mice were administered rAAV6 vectors via intramuscular
503 injections into the anterior and posterior compartments of the hind limbs. Each
504 compartment of the left limb received 2 x $10^{10}$ vector genomes (vg) of empty rAAV6, whilst
505 each compartment of the right limb received 1 x $10^{10}$ vg of WT HDAC4 AAV6 and 1 x $10^{10}$ vg
506 of WT HDAC5 AAV6. For expression of individual HDACs in gene dosage experiments, AAV
507 doses were administered as indicated in relevant Figures. Experiments with C57Bl6 mice
508 were performed 2-3 weeks after AAV administration. *db/db* mice were similarly

509 administered rAAV6 vectors via intramuscular injections into the anterior and posterior
510 compartments of the hind limbs. Each compartment of the left limb received 5 x $10^{10}$ vg of
511 empty rAAV6, whilst each muscle of the right limb received 2.5 x $10^{10}$ vg of DN HDAC4 AAV6
512 and 2.5 x $10^{10}$ vg of DN HDAC5 AAV6. Approximately 8 weeks after rAAV6 administration,
513 *db/db* mice were fasted for 4 hours before humane killing by cervical dislocation. Tissues
514 were rapidly excised and snap frozen in liquid nitrogen or fixed in 10% formalin.
515
516 **Respiration and mitochondrial function analysis**
517 Cells were treated with vehicle (BSA) or palmitate in 75$cm^2$ flasks for 24 hrs and transferred
518 to a 24-well XF24 microplate (Seahorse Bioscience) at 50,000 cells/well, with analysis
519 performed 3 hrs later. Mitochondrial function was assessed as previously described[54] and
520 respiratory analysis of skeletal muscle biopsies was also performed as previously
521 described[20].
522
523 **Lipidomics, metabolomics and acetyl-CoA analysis**
524 To determine cellular lipid profiles, ~1x$10^6$ cells were collected in 100µl of PBS and frozen at
525 -80°C, or ~10mg of muscle was homogenised in 100µl of PBS, and lipids were determined as
526 previously described[55]. Briefly, lipids were extracted using 20 volumes of
527 chloroform:methanol (2:1) in a single phase extraction process, recovering all lipids in a
528 single phase suitable for liquid chromatography–mass spectrometry analysis. Lipids were
529 identified using a HP 1200 liquid chromatography system (Agilent Technologies) coupled to
530 a PE Sciex API 4000 Q/TRAP mass spectrometer (Applied Biosystems/MDS SCIEX, Mulgrave,
531 VIC, Australia) with a turbo-ionspray source (350°C) and Analyst 1.5 data system (Applied
532 Biosystems/MDS SCIEX). Quantification of individual lipid species was performed using
533 multiple-reaction monitoring (MRM) in positive ion mode. MRM product ions used were
534 m/z 264 for ceramides, while diacylglycerides and triacylglycerides were monitored by the
535 neutral loss of individual fatty acid species. Each ion pair was monitored for between 10 and
536 50 ms (using scheduled MRM mode), with a resolution of 0.7 amu at half-peak height, and
537 averaged from continuous scans over the elution period. The proportionately higher signals
538 resulting from diacylglycerol and triacylglycerol consisting of two or more identical fatty
539 acids were corrected prior to normalisation against internal standards. Lipid concentrations
540 were calculated by relating the peak area of each species to the peak area of the
541 corresponding internal standards (100 pmol ceramide 17:0, 200 pmol diacylglycerol
542 17:0/17:0 and 100 pmol triacylglycerol 17:0/17:0/17:0), which were added prior to
543 extraction.
544
545 For metabolite and acetyl-CoA analysis, cells in 6-well plates underwent metabolic arrest by
546 washing in 1mL ultrapure water before being frozen instantaneously by the addition of
547 liquid nitrogen. To extract polar metabolites, 600µl of ice-cold 9:1 methanol:chloroform
548 containing internal standards (0.5nM 13C-sorbitol and 5nM 13C, 15N-valine) was added per
549 well. Following collection, samples were centrifuged at 16,000 x g for 5min at 4°C and the
550 supernatant stored at -80°C. Polar metabolites in cellular extracts, including acetyl-CoA,
551 were assessed using LC and high resolution QTOF mass spectrometry previously described [56]
552 with the following modifications. Samples (10µL) were injected onto an Agilent 1290 LC
553 fitted with a SeQuant ZIC®-pHILIC column (2.1 x 150 mm, 5µm; Merck) using 20mM
554 ammonium carbonate, pH 9.0 (Sigma-Aldrich) (A) and 100% acetonitrile (B) as the mobile
555 phases. The solvent flow rate of 250 µl/min and a 14 min gradient starting from 90% B to

556 40% B over 12 minutes, held for 2 min followed by washing at 5% B for 3 minutes and re-
557 equilibration at 90% B, was used.
558 **Microarray and gene expression analysis**
559 For cell culture studies, RNA was extracted from ~1 x $10^6$ cells. For comparative
560 transcriptomics analysis, RNA was also extracted from ~10mg of muscle from male
561 heterozygous db/+ and homozygous *db/db* mice. Each treatment group consisted of three
562 biological replicates and microarray analysis was performed as previously described[20]. For
563 comparative transcriptomics analyses between cell culture and mouse data, genes found to
564 be significantly altered in both data sets in the same direction (n = 236) were analysed by
565 gene set enrichment analysis from all KEGG pathway lists. The microarray datasets
566 generated conforms to MIAME guidelines and is available at Gene Expression Omnibus
567 (http://www.ncbi.nlm.nih.gov/geo/query/acc.cgi) series record GSE215185. Gene
568 expression was measured using real time RT-PCR as previously described [27]. Primer
569 sequences are available in Table S1.
570
571 **Protein fractionation, immunoprecipitation and western blot analysis**
572 Cells were collected in lysis buffer (50mM Tris pH 7.5, 1mM EDTA, 1mM EGTA, 10% glycerol,
573 1% Triton X-100, 50mM NaF, 5mM sodium pyrophosphate, 1mM DTT, 1X protease inhibitor
574 cocktail (Sigma)) and ~20mg skeletal muscle was homogenised in 10v volume of lysis buffer
575 using a handheld homogeniser. Protein concentration was determined using the BCA assay
576 (Pierce). Fractionation procedures, immunoprecipitation and western blotting were
577 performed as previously described[57]. Antibody details are listed in Table S2.
578
579 **Stable isotope metabolomics and insulin and isotopic glucose administration**
580 To assess insulin action, mice were administered 200uCi/kg body weight of 2[1,2-$^3$H]-
581 deoxyglucose and 100uCi/kg body weight of 1-$^{14}$C glucose, with or without 1.2U/kg
582 bodyweight of insulin after a 5hr fast. Blood glucose was determined using a handheld
583 glucometer (Accu-Chek Performa, Roche) and ~5µL blood was obtained from the tail tip
584 prior to tracer administration and 5, 15 and 30min after tracer administration. Collected
585 blood was mixed with 75ul of a 2.5% zinc sulfate solution in 1.5ml tubes before being stored
586 on ice. Mice were humanely killed by cervical dislocation 30 min after tracer administration
587 and tissues were collected. At the conclusion of the test 25µl of saturated 0.3N barium
588 hydroxide was added to the blood samples. The samples where then mixed by pipetting
589 before centrifugation at 1000 x g for 5 min at 4$^o$C to pellet any precipitated protein. After
590 centrifugation 25µl of supernatant was transferred to scintillation vials containing 2ml of
591 Ultima Gold scintillation liquid (Perkin Elmer) before $^3$H and$^{14}$C counts were measured on a
592 beta counter (Tri-Carb 2910TR, Perkin Elmer) to determine blood tracer concentration. The
593 tibialis anterior (TA) skeletal muscle (15-25mg) was used to determine 2-deoxyglucose
594 clearance as we have previously described[58]. To determine 1-$^{14}$C glucose incorporation into
595 glycogen, ~10-15mg of TA muscle was digested in 1M KOH at 70$^o$C for 20 min and glycogen
596 was precipitated with saturated $Na_2SO_4$, washed twice with 95% ethanol and resuspended
597 in acetate buffer (0.84% sodium acetate, 0.46% acetic acid, pH 4.75) containing 0.3mg/mL
598 amyloglucosidase (Sigma). Glycogen was allowed to digest overnight at 37$^o$C before being
599 assayed for glucose content using the glucose oxidase method[54]. Digested glycogen was also
600 assessed for $^{14}$C-glucose incorporation by scintillation counting. To determine 1-$^{14}$C glucose
601 incorporation into lipids, 5-10mg of TA muscle was homogenised in chloroform/methanol
602 (2:1) and mixed overnight at room temperature. Organic and inorganic phases were

603 separated by addition of 0.6% NaCl and the lower organic phase was collected and
604 evaporated under $N_2$ at 45$^{o}$C. The dried extract was resuspended in absolute ethanol and TG
605 content was assayed using TG GPO-PAP reagent (Roche) and $^{14}$C-glucose incorporation by
606 scintillation counting.
607
608 To assess oxidative glucose utilisation, mice were administered a bolus of 50mg of [U-$^{13}$C]
609 glucose (Sigma-Aldrich) via oral gavage. At 60 min after [U-$^{13}$C] glucose administration, mice
610 were humanely killed by cervical dislocation and skeletal muscles were immediately
611 collected. Targeted metabolomic analysis with [U-$^{13}$C] glucose was performed as we have
612 previously described[58]. Briefly, approximately 25-30mg of mixed gastrocnemius muscle
613 tissue was homogenised in 1.2mL of 3:1 methanol:d$H_2O$ (-15$^{o}$C) using a bead cryomill
614 (Precellys). Extracted metabolites were derivatised before injection into an gas
615 chromatography system (Agilent 6890N) connected to a VF-5ms capillary column with a 10-
616 m inert EZ-guard (30m, 0.25mm, 0.25µm) and mass selective detector (Agilent 5975C) with
617 helium as the carrier gas. Electron ionisation mode was used for the measurement of all
618 organic and amino acids in their TBDMS derivatized form via analysis of their pseudo-
619 molecular fragment ions (i.e. M-57). All metabolites were analysed in the selected ion
620 monitoring mode. Ion abundances, measured as the area under the chromatogram curve,
621 were determined using the Mass Hunter Workstation (Agilent Technologies, Mulgrave,
622 Australia). Total metabolite labelling in HDAC4 and 5 over expressing muscle was expressed
623 relative to labelling in the control muscle within each mouse.
624
625 **Measurement of apoptosis and cell viability**.
626 Analysis of apoptotic cells was performed by dual staining with FITC-conjugated Annexin V
627 (BD Pharmingen) and propidium iodide (PI; Molecular Probes) and was optimised for
628 adherent cells. Cells in 12-well plates were rinsed with PBS containing 2mM EDTA and
629 removed from the culture plate using 0.025% trypsin in PBS/2mM EDTA. Trypsin was
630 inactivated using growth media containing an extra 10% FBS and centrifuged at 500g for
631 5min. Cells were resuspended and incubated in growth media for ~1h. Staining was
632 performed in growth media using 5.0µg/mL PI and FITC-conjugated Annexin V according to
633 the manufacturer's protocol and incubated for 15min in the dark. Annexin binding buffer
634 (250µl, 10mM HEPES pH 7.4, 140mM NaCl, 2.5mM $CaCl_2$) was added and cells were
635 immediately analysed by flow cytometry to determine the percentage of viable (Annexin $V^-$
636 /$PI^-$) and early apoptotic (Annexin $V^+$/$PI^-$) cells. For measurement of apoptosis in tissues,
637 caspase 3 activity was measured using Caspase-Glo 3/7 assay (Promega,) from
638 approximately 10mg of EDL tissue from *db/db* mice administered rAAVs.
639
640 Detection of absolute non-viable cells was performed by staining with 7-aminoactinomycin
641 D (7-AAD; BD Pharmingen) and flow cytometry, with crystal violet staining and colorimetric
642 detection, or by LDH release depending on the model used. For 7AAD staining, cells in a 12-
643 well plate were dislodged with 0.125% trypsin in phosphate buffered saline (PBS) containing
644 5mM EDTA, centrifuged at 500g for 5min and resuspended in 100µl PBS with 0.2% bovine
645 serum albumin (BSA). Staining was performed by adding 10µl 7-AAD and incubating in the
646 dark for 10min. Cells were then rinsed with PBS and fixed in 1% paraformaldehyde
647 supplemented with 2% FBS and 2µg/ml actinomycin D before being analysed by flow
648 cytometry using the FACS Calibur® system. The percentage of viable (7-$AAD^-$) and
649 apoptotic/necrotic (7-$AAD^+$ non-viable) cells was determined using BD CellQuest™ Pro

650 software (BD Biosciences). For detection of relative non-viable cells, crystal violet staining
651 was performed as we have previously described[59] and cell viability was represented relative
652 to vehicle treated cells. For myotube experiments, cell viability was assessed by LDH release
653 and represented relative to total cellular LDH, as we have previously described[54].
654
655 **$^{14}$C-incorporation from palmitate and glucose into p53.**
656 Cells in a 6-well culture plate were washed twice with PBS and incubated with D-
657 [$^{14}$C]Glucose (1.14µCi/well; PerkinElmer) or [$^{14}$C]Palmitic Acid (0.5µCi/well; PerkinElmer) in
658 growth media for 3 hr. Immunoprecipitation of FLAG-tagged p53 was performed with anti-
659 FLAG tag antibody (Cell Signaling). Beads were washed multiple times with ice cold PBS and
660 half of the beads were analysed by scintillation counting. The remaining beads were
661 resuspended in Lane Marker Reducing Sample Buffer (Pierce) and proteins analysed by
662 western blotting. Scintillation counts were normalised to the p53 protein in each
663 immunoprecipitation.
664
665 **Reactive oxygen species detection**
666 In cells, hydrogen peroxide ($H_2O_2$) was detected using Amplex Red assay (Invitrogen).
667 Briefly, cells were seeded into a 96-well plate at a density of 25,000 cells per well. The
668 following day, cells were treated with vehicle (DMSO), 100µM mitoTEMPO or 100µM
669 apocynin for 30 min at 37°C. Cells were then co-incubated with 50µM Amplex Red and
670 0.1U/ml horseradish peroxidase (HRP) for a further 30 min at 37°C. Production of the
671 fluorescent product resorufin was detected on a Flexstation II$^{384}$ fluorometer (Molecular
672 Devices; excitation 544nm, emission 590nm). Mitochondrial ROS was designated as that
673 sensitive to MitoTEMPO, while NADPH oxidase ROS was designated as that sensitive to
674 apocynin. For tissues, the OxiSelect In Vitro ROS/RNS Assay kit (Green Fluorescence) (Cell
675 Biolabs Inc.) was used according to the manufacturer's instructions, using lysates from
676 homogenised extensor digitorum longus (EDL) muscle from *db/db* mice. The assay was
677 performed in a black 96-well plate with DCF standards and was read on a fluorometer
678 (Flexstation II$^{384}$ Molecular Devices; excitation 480nm, emission 530nm).
679
680 **GPX4 activity and lipid peroxidation**
681 To measure glutathione dependent peroxidase activity within cultured cells and skeletal
682 muscle, a Glutathione Peroxidase Assay Kit (colorimetric) (Ab Cam Australia) was used. A
683 modified method of the standard protocol was used in both cells and tissue. Cells were
684 plated into 10cm tissue culture plates at 4 X $10^6$ cells per dish. After 3hrs the growth media
685 was refreshed and cells incubated for 1hr, washed and collected in 250ul of the supplied
686 assay buffer. For tissues, lysate from homogenised gastrocnemius muscle from *db/db* mice
687 was analysed. The assay was performed according to manufacturer's instructions, including
688 generation of the NADPH standards. The reaction was incubated at room temp for 15min.
689 The plate was then read on a plate reader at 340nm (Xmark, Bio-Rad) to ensure all samples
690 had an OD above 1 but below the OD of the highest standard. Next 10ul of cumene
691 hydroperoxide was added to each of the sample and reagent control wells, mixed and the $T_1$
692 reading taken at 340nm. Following this the plate was incubated in the plate reader at 25$^o$C
693 for 5mins then the $T_2$ reading was taken again at 340nm. Data was then analyzed as
694 described by the manufacturer with all results being normalized to protein concentration.
695

696 Lipid peroxidation in both cells and muscle lysates was assessed using a lipid peroxidation
697 kit (Sigma). Approximately 1 x $10^6$ cells were collected in MDA lysis buffer while lysate from
698 homogenised gastrocnemius muscle from *db/db* mice was analysed. The assay was
699 performed according to manufacturer's instructions, including addition of butanol to the
700 reaction.
701
702 **Histology**
703 Fixed TA muscles from db/db mice were processed by University of Melbourne Histology.
704 Tissues were embedded in paraffin before transverse sections were obtained at 5µm
705 thickness and stained for H&E and Masson's trichrome. Slides were imaged with a slide
706 scanner (Aperio, Leica Biosystems). Images were analysed using photoshop and image J to
707 quantify fibre diameter and cell number.
708
709 **Statistical analysis.**
710 All data are expressed as mean ± SEM. Individual data points identified as greater than two
711 standard deviations away from the mean were designated as outliers and removed from the
712 dataset. Data was assessed for normality using the Shapiro-Wilk test. Differences between
713 groups were assessed using t-test, Kruskal-Wallis test, one-way ANOVA or two-way ANOVA
714 as appropriate using GraphPad Prism. Specific differences between groups were identified
715 using Dunn's or Tukey's multiple comparisons tests. For animal experiments where
716 opposing hind limbs were administered different rAAVs, such that control and experimental
717 conditions were contained within the one animal, paired t-tests were used. Differences
718 were considered statistically significant where $p<0.05$.

## ACKNOWLEDGEMENTS

The authors wish to thank all members of the Metabolic Reprogramming Laboratory for helpful insights and technical advice and are grateful to the technical staff of the Deakin University Animal Services team. The authors also wish to thank Hongwei Qian for AAV production. This work was supported by grants from the National Health and Medical Research Council (NHMRC: APP1027227, APP1030474 and APP1127059) to SLM. PJM, PG and MAF are supported by Fellowships from the NHMRC.

## AUTHOR CONTRIBUTIONS

Conceptualization, SDM, TC and SLM; Methodology, SDM, TC, DDS, GMK, CRB, PG, FMC, KRW and SLM; Investigation, SDM, TC, AS, KAM, DCH, BN, DDS, GMK, FMC and SLM; Resources, DLT, PJM, CRB, PG, MAF and SLM; Writing – original draft, SDM, TC and SLM; Writing – review and editing, all authors; Funding acquisition, SLM.

## DECLARATION OF INTERESTS

The authors declare no competing interests related to this article.

## SUPPLEMENTARY FILES

- MDAR checklist
- Supplementary tables file

## DATA AND MATERIALS AVAILABILITY

All data generated during this study are included in data supplement files. Microarray datasets are available at Gene Expression Omnibus (http://www.ncbi.nlm.nih.gov/geo/query/acc.cgi) series record GSE215185. Any unique or newly created materials will be made available upon request wherever possible.

749 **REFERENCES**
750

751 1. Lee Y, Hirose H, Ohneda M, Johnson JH, McGarry JD, Unger RH. Beta-cell lipotoxicity
752 in the pathogenesis of non-insulin-dependent diabetes mellitus of obese rats:
753 impairment in adipocyte-beta-cell relationships. *Proceedings of the National*
754 *Academy of Sciences of the United States of America* **91**, 10878-10882 (1994).
755
756 2. Schaffer JE. Lipotoxicity: when tissues overeat. *Current opinion in lipidology* **14**, 281-
757 287 (2003).
758
759 3. Montgomery MK, De Nardo W, Watt MJ. Impact of Lipotoxicity on Tissue "Cross
760 Talk" and Metabolic Regulation. *Physiology* **34**, 134-149 (2019).
761
762 4. Listenberger LL*, et al.* Triglyceride accumulation protects against fatty acid-induced
763 lipotoxicity. *Proceedings of the National Academy of Sciences of the United States of*
764 *America* **100**, 3077-3082 (2003).
765
766 5. Kelley DE, Simoneau JA. Impaired free fatty acid utilization by skeletal muscle in non-
767 insulin-dependent diabetes mellitus. *The Journal of clinical investigation* **94**, 2349-
768 2356 (1994).
769
770 6. Simoneau JA, Kelley DE. Altered glycolytic and oxidative capacities of skeletal muscle
771 contribute to insulin resistance in NIDDM. *Journal of applied physiology* **83**, 166-171
772 (1997).
773
774 7. Baker PR, 2nd*, et al.* Metabolomic analysis reveals altered skeletal muscle amino acid
775 and fatty acid handling in obese humans. *Obesity (Silver Spring)* **23**, 981-988 (2015).
776
777 8. Lerin C*, et al.* Defects in muscle branched-chain amino acid oxidation contribute to
778 impaired lipid metabolism. *Molecular metabolism* **5**, 926-936 (2016).
779
780 9. White PJ*, et al.* Branched-chain amino acid restriction in Zucker-fatty rats improves
781 muscle insulin sensitivity by enhancing efficiency of fatty acid oxidation and acyl-
782 glycine export. *Molecular metabolism* **5**, 538-551 (2016).
783
784 10. Muoio DM, Neufer PD. Lipid-induced mitochondrial stress and insulin action in
785 muscle. *Cell metabolism* **15**, 595-605 (2012).
786
787 11. Sparks LM*, et al.* A high-fat diet coordinately downregulates genes required for
788 mitochondrial oxidative phosphorylation in skeletal muscle. *Diabetes* **54**, 1926-1933
789 (2005).
790
791 12. Patti ME*, et al.* Coordinated reduction of genes of oxidative metabolism in humans
792 with insulin resistance and diabetes: Potential role of PGC1 and NRF1. *Proceedings of*
793 *the National Academy of Sciences of the United States of America* **100**, 8466-8471
794 (2003).

795

796 13. Zechner C*, et al.* Total skeletal muscle PGC-1 deficiency uncouples mitochondrial
797 derangements from fiber type determination and insulin sensitivity. *Cell metabolism*
798 **12**, 633-642 (2010).
799
800 14. Choi CS*, et al.* Paradoxical effects of increased expression of PGC-1alpha on muscle
801 mitochondrial function and insulin-stimulated muscle glucose metabolism.
802 *Proceedings of the National Academy of Sciences of the United States of America*
803 **105**, 19926-19931 (2008).
804
805 15. Dube JJ*, et al.* Effects of acute lipid overload on skeletal muscle insulin resistance,
806 metabolic flexibility, and mitochondrial performance. *American journal of physiology*
807 *Endocrinology and metabolism* **307**, E1117-1124 (2014).
808
809 16. Richardson DK*, et al.* Lipid infusion decreases the expression of nuclear encoded
810 mitochondrial genes and increases the expression of extracellular matrix genes in
811 human skeletal muscle. *The Journal of biological chemistry* **280**, 10290-10297 (2005).
812
813 17. Staiger H, Staiger K, Haas C, Weisser M, Machicao F, Haring HU. Fatty acid-induced
814 differential regulation of the genes encoding peroxisome proliferator-activated
815 receptor-gamma coactivator-1alpha and -1beta in human skeletal muscle cells that
816 have been differentiated in vitro. *Diabetologia* **48**, 2115-2118 (2005).
817
818 18. Coll T*, et al.* Palmitate-mediated downregulation of peroxisome proliferator-
819 activated receptor-gamma coactivator 1alpha in skeletal muscle cells involves
820 MEK1/2 and nuclear factor-kappaB activation. *Diabetes* **55**, 2779-2787 (2006).
821
822 19. Crunkhorn S*, et al.* Peroxisome proliferator activator receptor gamma coactivator-1
823 expression is reduced in obesity: potential pathogenic role of saturated fatty acids
824 and p38 mitogen-activated protein kinase activation. *The Journal of biological*
825 *chemistry* **282**, 15439-15450 (2007).
826
827 20. Gaur V*, et al.* Disruption of the Class IIa HDAC Corepressor Complex Increases Energy
828 Expenditure and Lipid Oxidation. *Cell reports* **16**, 2802-2810 (2016).
829
830 21. Czubryt MP, McAnally J, Fishman GI, Olson EN. Regulation of peroxisome
831 proliferator-activated receptor gamma coactivator 1 alpha (PGC-1 alpha ) and
832 mitochondrial function by MEF2 and HDAC5. *Proceedings of the National Academy*
833 *of Sciences of the United States of America* **100**, 1711-1716 (2003).
834
835 22. Backs J, Backs T, Bezprozvannaya S, McKinsey TA, Olson EN. Histone deacetylase 5
836 acquires calcium/calmodulin-dependent kinase II responsiveness by oligomerization
837 with histone deacetylase 4. *Molecular and cellular biology* **28**, 3437-3445 (2008).
838
839 23. Lemercier C, Verdel A, Galloo B, Curtet S, Brocard MP, Khochbin S. mHDA1/HDAC5
840 histone deacetylase interacts with and represses MEF2A transcriptional activity. *The*
841 *Journal of biological chemistry* **275**, 15594-15599 (2000).
842

24. McKinsey TA, Zhang CL, Lu J, Olson EN. Signal-dependent nuclear export of a histone deacetylase regulates muscle differentiation. *Nature* **408**, 106-111 (2000).

25. McGee SL*, et al.* AMP-activated protein kinase regulates GLUT4 transcription by phosphorylating histone deacetylase 5. *Diabetes* **57**, 860-867 (2008).

26. Mihaylova MM*, et al.* Class IIa histone deacetylases are hormone-activated regulators of FOXO and mammalian glucose homeostasis. *Cell* **145**, 607-621 (2011).

27. McGee SL*, et al.* Compensatory regulation of HDAC5 in muscle maintains metabolic adaptive responses and metabolism in response to energetic stress. *FASEB journal : official publication of the Federation of American Societies for Experimental Biology* **28**, 3384-3395 (2014).

28. McGee SL, Fairlie E, Garnham AP, Hargreaves M. Exercise-induced histone modifications in human skeletal muscle. *The Journal of physiology* **587**, 5951-5958 (2009).

29. Petersen KF, Dufour S, Befroy D, Garcia R, Shulman GI. Impaired mitochondrial activity in the insulin-resistant offspring of patients with type 2 diabetes. *The New England journal of medicine* **350**, 664-671 (2004).

30. Kowalski GM*, et al.* Application of dynamic metabolomics to examine in vivo skeletal muscle glucose metabolism in the chronically high-fat fed mouse. *Biochemical and biophysical research communications* **462**, 27-32 (2015).

31. Zhang W, Guo C, Jiang K, Ying M, Hu X. Quantification of lactate from various metabolic pathways and quantification issues of lactate isotopologues and isotopmers. *Sci Rep* **7**, 8489 (2017).

32. Ryan DG*, et al.* Disruption of the TCA cycle reveals an ATF4-dependent integration of redox and amino acid metabolism. *Elife* **10**, (2021).

33. Jiang X, Stockwell BR, Conrad M. Ferroptosis: mechanisms, biology and role in disease. *Nature reviews Molecular cell biology* **22**, 266-282 (2021).

34. Sykes SM*, et al.* Acetylation of the p53 DNA-binding domain regulates apoptosis induction. *Molecular cell* **24**, 841-851 (2006).

35. Tang Y, Luo J, Zhang W, Gu W. Tip60-dependent acetylation of p53 modulates the decision between cell-cycle arrest and apoptosis. *Molecular cell* **24**, 827-839 (2006).

36. Sen N, Kumari R, Singh MI, Das S. HDAC5, a key component in temporal regulation of p53-mediated transactivation in response to genotoxic stress. *Molecular cell* **52**, 406-420 (2013).

889 37. Jiang L*, et al.* Ferroptosis as a p53-mediated activity during tumour suppression.
890 *Nature* **520**, 57-62 (2015).
891
892 38. Berkers CR, Maddocks OD, Cheung EC, Mor I, Vousden KH. Metabolic regulation by
893 p53 family members. *Cell metabolism* **18**, 617-633 (2013).
894
895 39. Lahm A*, et al.* Unraveling the hidden catalytic activity of vertebrate class IIa histone
896 deacetylases. *Proceedings of the National Academy of Sciences of the United States*
897 *of America* **104**, 17335-17340 (2007).
898
899 40. Martinez-Reyes I, Chandel NS. Mitochondrial TCA cycle metabolites control
900 physiology and disease. *Nature communications* **11**, 102 (2020).
901
902 41. Berwick DC, Hers I, Heesom KJ, Moule SK, Tavare JM. The identification of ATP-
903 citrate lyase as a protein kinase B (Akt) substrate in primary adipocytes. *The Journal*
904 *of biological chemistry* **277**, 33895-33900 (2002).
905
906 42. Stockwell BR*, et al.* Ferroptosis: A Regulated Cell Death Nexus Linking Metabolism,
907 Redox Biology, and Disease. *Cell* **171**, 273-285 (2017).
908
909 43. Kagan VE*, et al.* Oxidized arachidonic and adrenic PEs navigate cells to ferroptosis.
910 *Nature chemical biology* **13**, 81-90 (2017).
911
912 44. Ou Y, Wang SJ, Li D, Chu B, Gu W. Activation of SAT1 engages polyamine metabolism
913 with p53-mediated ferroptotic responses. *Proceedings of the National Academy of*
914 *Sciences of the United States of America* **113**, E6806-E6812 (2016).
915
916 45. Piccolis M*, et al.* Probing the Global Cellular Responses to Lipotoxicity Caused by
917 Saturated Fatty Acids. *Molecular cell* **74**, 32-44 e38 (2019).
918
919 46. Turpin SM*, et al.* Examination of 'lipotoxicity' in skeletal muscle of high-fat fed and
920 ob/ob mice. *The Journal of physiology* **587**, 1593-1605 (2009).
921
922 47. Murphy MP, Chouchani ET. Why succinate? Physiological regulation by a
923 mitochondrial coenzyme Q sentinel. *Nature chemical biology* **18**, 461-469 (2022).
924
925 48. Burger N*, et al.* A sensitive mass spectrometric assay for mitochondrial CoQ pool
926 redox state in vivo. *Free radical biology & medicine* **147**, 37-47 (2020).
927
928 49. Chance B, Hollunger G. The interaction of energy and electron transfer reactions in
929 mitochondria. I. General properties and nature of the products of succinate-linked
930 reduction of pyridine nucleotide. *The Journal of biological chemistry* **236**, 1534-1543
931 (1961).
932
933 50. Mills EL*, et al.* Succinate Dehydrogenase Supports Metabolic Repurposing of
934 Mitochondria to Drive Inflammatory Macrophages. *Cell* **167**, 457-470 e413 (2016).
935

936 51. Mills EL*, et al.* Accumulation of succinate controls activation of adipose tissue
937 thermogenesis. *Nature* **560**, 102-106 (2018).
938
939 52. Fernandez-Aguera MC*, et al.* Oxygen Sensing by Arterial Chemoreceptors Depends
940 on Mitochondrial Complex I Signaling. *Cell metabolism* **22**, 825-837 (2015).
941
942 53. Winbanks CE*, et al.* The bone morphogenetic protein axis is a positive regulator of
943 skeletal muscle mass. *The Journal of cell biology* **203**, 345-357 (2013).
944
945 54. Martin SD, Morrison S, Konstantopoulos N, McGee SL. Mitochondrial dysfunction has
946 divergent, cell type-dependent effects on insulin action. *Molecular metabolism* **3**,
947 408-418 (2014).
948
949 55. Genders AJ*, et al.* Reducing hepatic PKD activity lowers circulating VLDL cholesterol. *J*
950 *Endocrinol* **246**, 265-276 (2020).
951
952 56. Hortle E*, et al.* Adenosine monophosphate deaminase 3 activation shortens
953 erythrocyte half-life and provides malaria resistance in mice. *Blood* **128**, 1290-1301
954 (2016).
955
956 57. McGee SL, Hargreaves M. Exercise and myocyte enhancer factor 2 regulation in
957 human skeletal muscle. *Diabetes* **53**, 1208-1214 (2004).
958
959 58. De Jong KA*, et al.* Loss of protein kinase D activity demonstrates redundancy in
960 cardiac glucose metabolism and preserves cardiac function in obesity. *Molecular*
961 *metabolism* **42**, 101105 (2020).
962
963 59. Preston S*, et al.* 1-Methyl-1H-pyrazole-5-carboxamide Derivatives Exhibit
964 Unexpected Acute Mammalian Toxicity. *Journal of medicinal chemistry* **64**, 840-844
965 (2021).
966
967
968
969
970

**FIGURE 1**

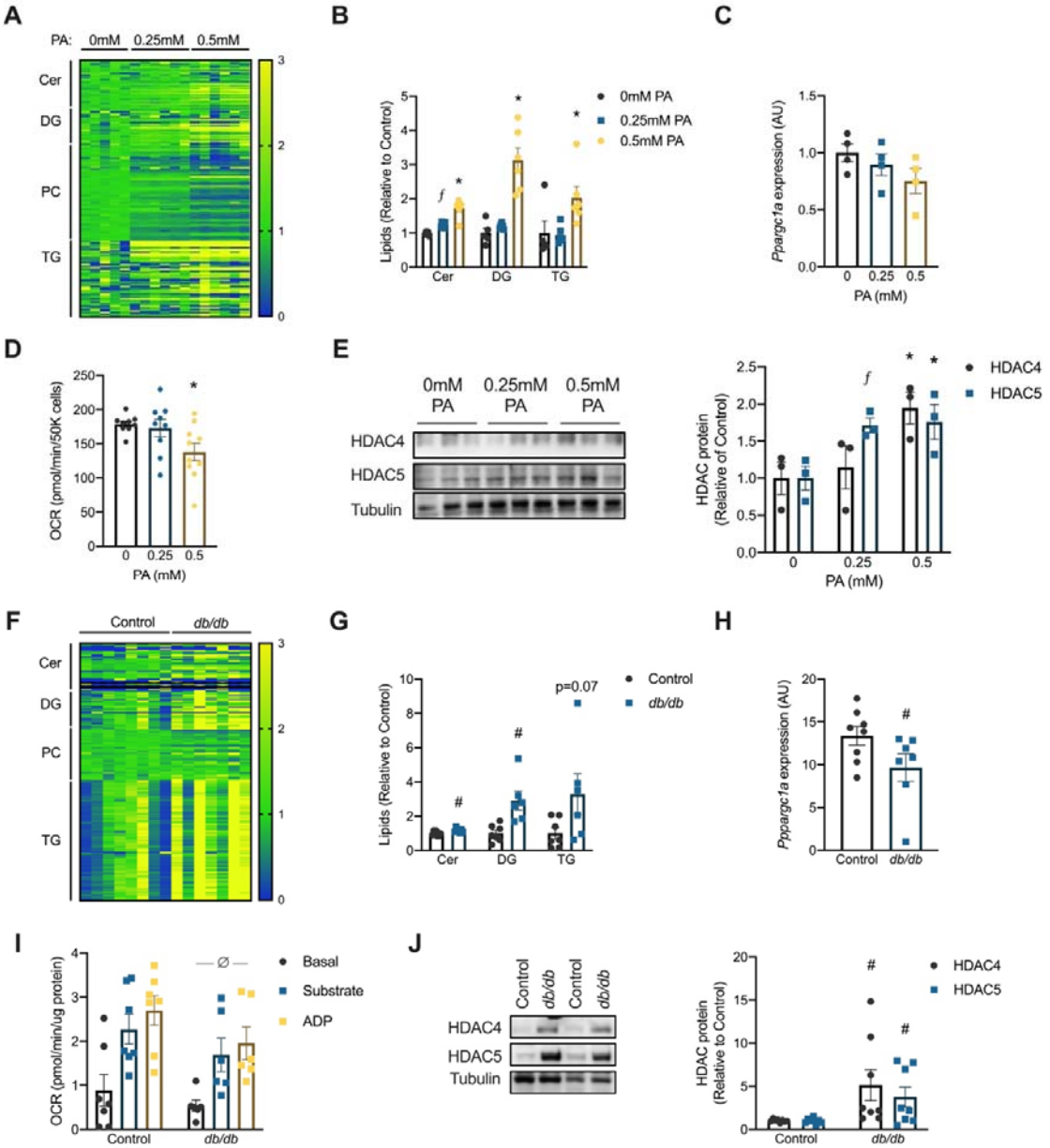


**Figure 1: HDAC4 and 5 are increased in models of lipotoxicity.** (A) Heat map of ceramide (Cer), diglyceride (DG), phosphatidylcholine (PC) and triglyceride (TG) lipid species; (B) Total Cer, DG and TG lipids (One-way ANOVA; Cer $p<0.0001$ ($F(2,14)=73.86$, $^{f}$Tukey's multiple comparisons test $p<0.0077$ vs. 0mM, *Tukey's multiple comparisons test $p<0.0001$ vs. 0mM and vs 0.25mM; DG $p<0.0001$ ($F(2,14)=38.50$ *Tukey's multiple comparisons test $p<0.0001$ vs. 0mM and vs 0.25mM; TG $p<0.0017$ ($F(2,14)=10.38$ *Tukey's multiple comparisons test $p=0.0333$ vs. 0mM); (C) *Ppargc1a* gene expression; (D) Oxygen consumption rate (OCR; One-way ANOVA $p<0.0255$ ($F(2,25)=4.262$ *Tukey's multiple comparisons test $p<0.0001$ vs. 0mM and vs 0.25mM), and; (E) HDAC4 and 5 protein in C2C12 myotubes treated with 0mM (BSA vehicle), 0.25mM or 0.5mM palmitate (PA) for 24 hrs (HDAC4, Kruskal-Wallis test, $p=0.049$

($X^2$ = 5.591), *Dunn's multiple comparison test $p$=0.0380; HDAC5, One-way ANOVA, $p$=0.038 (F(2,6)=5.903) $^{f}$Tukey's multiple comparisons test $p$=0.0318, *Tukey's multiple comparisons test $p$=0.0251). (F) Heat map of Cer, DG, PC and TG lipid species; (G) Total Cer, DG and TG lipids (Unpaired t-tests, Cer $p$=0.0094, DG $p$=0.0022, TG $p$=0.0616); (H) *Ppargc1a* gene expression (Unpaired t-test, $p$=0.0357); (I) Basal, substrate and ADP-driven OCR from muscle biopsies (Two-way ANOVA, $^{\varnothing}$genotype $p$=0.0493, $F$(1,33)=4.166), and; (J) HDAC4 and 5 protein in Control and *db/db* mice (Mann-Whitney test, $^{\#}$HDAC4 $p$=0.0002, Unpaired t-test $^{\#}$HDAC5 $p$=0.0308). Data are mean±SEM, n=3-6 biological replicates per group for cell experiments and 6-8 per group for animal experiments.

**Figure 1 - source data 1:** Source data for Figure 1A

**Figure 1 - source data 2:** Source data for Figure 1B

**Figure 1 - source data 3:** Source data for Figure 1C

**Figure 1 - source data 4:** Source data for Figure 1D

**Figure 1 - source data 5:** Source data and raw blots for Figure 1E

**Figure 1 - source data 6:** Source data for Figure 1F

**Figure 1 - source data 7:** Source data for Figure 1G

**Figure 1 - source data 8:** Source data for Figure 1H

**Figure 1 - source data 9:** Source data for Figure 1I

**Figure 1 - source data 10:** Source data and raw blots for Figure 1J

**Figure 1 Supplement** – Viability and gene expression responses to lipotoxicity.

**Figure 1 supplement – source data 1:** Source data for Figure S1A

**Figure 1 supplement – source data 1:** Source data for Figure S1B

**Figure 1 supplement – source data 1:** Source data for Figure S1C

1027 **FIGURE 2**

1028

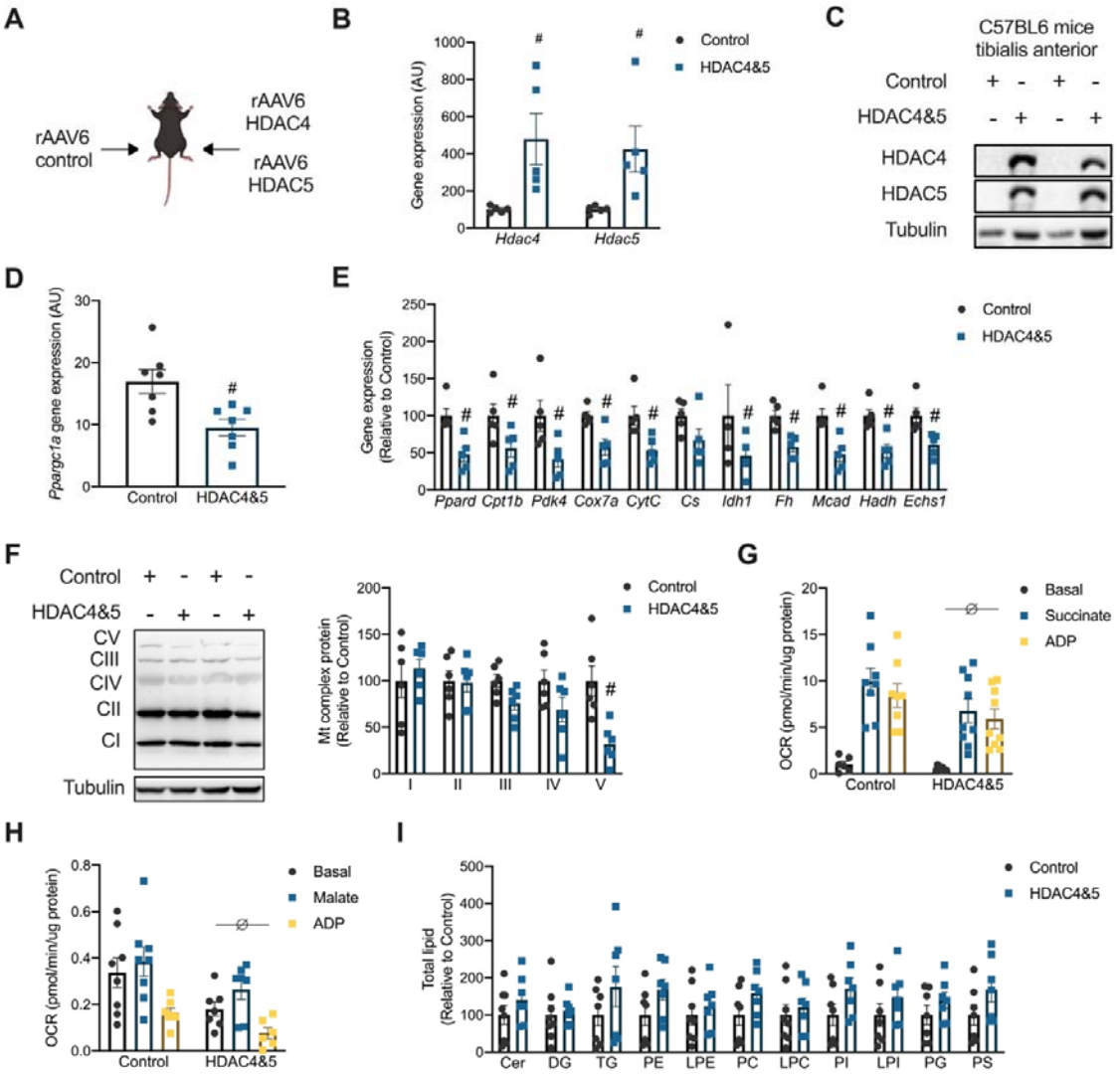


1029

1030 **Figure 2: Overexpression of HDAC4 and 5 in skeletal muscle suppresses *Pppargc1a***
1031 **expression and oxidative capacity.** (A) The bilateral AAV6 HDAC4 and 5 overexpression
1032 mouse model. (B) *Hdac4* and *Hdac5* gene expression (Paired t-test, #*Hdac4* $p$=0.0246,
1033 #*Hdac5* $p$=0.0305); (C) HDAC4 and 5 protein; (D) *Ppargc1a* gene expression (Paired t-test,
1034 $p$=0.0006); (E) Metabolic gene expression (Paired t-test, #*Ppard* $p$=0.0056, #*Cpt1b* $p$=0.0212,
1035 #*Pdk4* $p$=0.0058, #*Cox7a* $p$=0.0175, #*CytC* $p$=0.0042, #*Idh1* $p$=0.0358, #*Fh* $p$=0.0030, #*Mcad*
1036 $p$=0.0056, #*Hadh* $p$=0.0057, #*Echs1* $p$=0.0046); (F) Respiratory chain complex subunit protein
1037 (Paired t-test, #Complex V $p$=0.0036); (G) Basal, succinate and ADP-driven oxygen
1038 consumption rate (OCR) from muscle biopsies (Two-way ANOVA, ∅genotype $p$=0.0247,
1039 $F(1,43)=5.417$); (H) Basal, malate and ADP-driven OCR from muscle biopsies (Two-way
1040 ANOVA, ∅genotype $p$=0.0036, $F(1,37)=9.661$), and; (I) Ceramide (Cer), diglyceride (DG),
1041 triglyceride (TG), phosphatidylethanolamine (PE), lysophosphatidylethanolamine (LPE),
1042 phosphatidylcholine (PC), lysophosphatidylcholine (LPC), phosphatidylinositol (PI),
1043 lysophosphatidylinositol (LPI), phosphoglycerol (PG) and phosphatidylserine (PS) lipids in

Control and HDAC4 and 5 overexpressing skeletal muscle. Data are mean±SEM, n=4-6 per group.

**Figure 2 - source data 1:** Source data for Figure 2B

**Figure 2 - source data 2:** Raw blots for Figure 2C

**Figure 2 - source data 3:** Source data for Figure 2D

**Figure 2 - source data 4:** Source data for Figure 2E

**Figure 2 - source data 5:** Source data and raw blots for Figure 2F

**Figure 2 - source data 6:** Source data for Figure 2G

**Figure 2 - source data 7:** Source data for Figure 2H

**Figure 2 - source data 8:** Source data for Figure 2I

**Figure 2 Supplement** - Individual HDAC isoform and gene dosage effects on *Ppargc1a expression.*

**Figure 2 supplement – source data 1:** Source data for Figure S2B

**Figure 2 supplement – source data 2:** Raw blots for Figure S2C

**Figure 2 supplement – source data 3:** Source data for Figure S2D

**Figure 2 supplement – source data 4:** Source data for Figure S2E

1075 **FIGURE 3**

1076

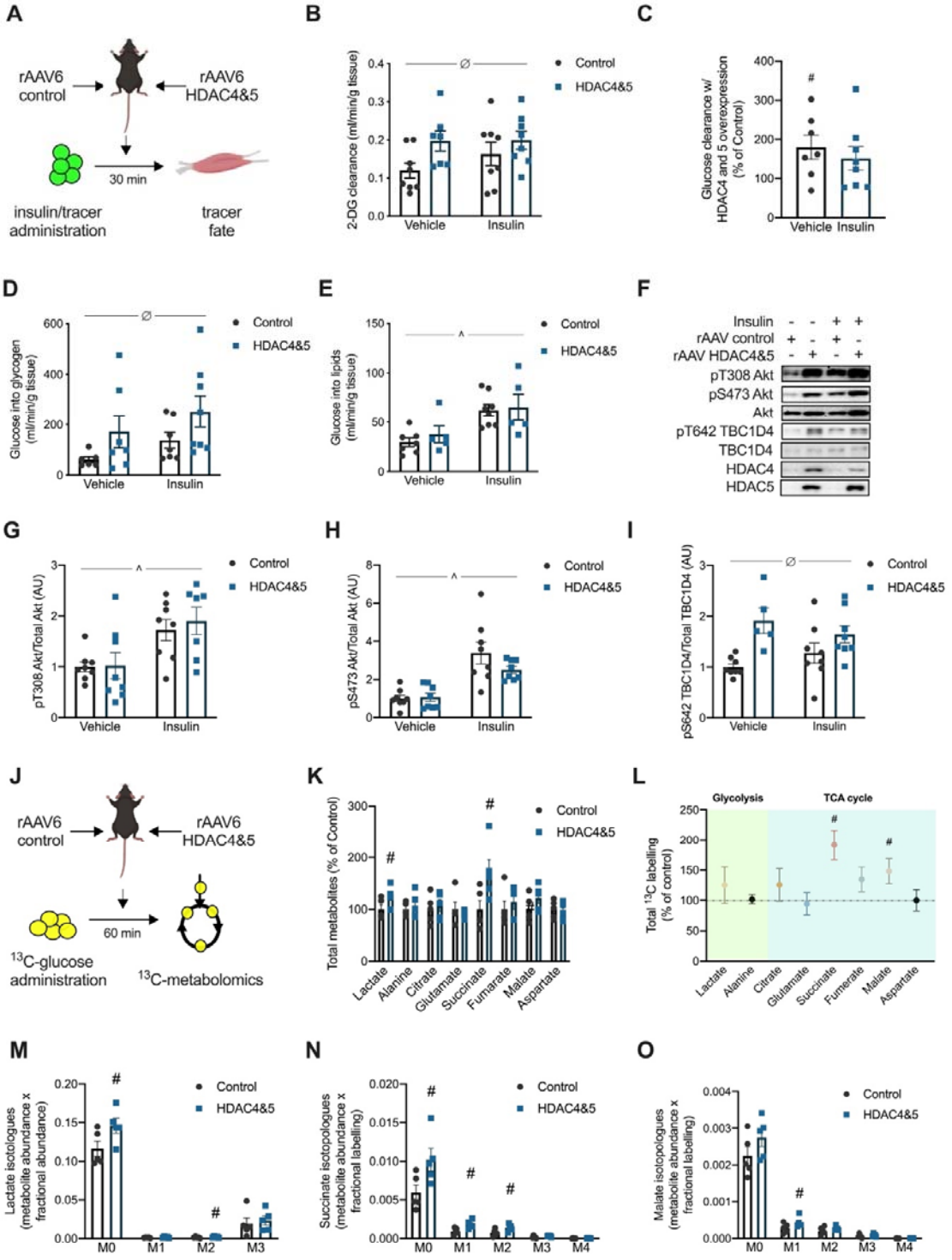


1077

1078

1079 **Figure 3: Overexpression of HDAC4 and 5 in skeletal muscle inhibits oxidative glucose**
1080 **utilisation.** (A) Experimental overview of insulin and isotopic glucose tracers in the bilateral
1081 AAV6 HDAC4 and 5 overexpression model. (B) Glucose clearance (Two-way ANOVA,
1082 ∅genotype $p$=0.0328, $F$(1,27)=5.061); (C) Glucose clearance in muscle overexpressing HDAC4

1083 and 5 relative to Control (Paired t-test, #Vehicle $p$=0.0355); (D) $^{14}$C-glucose incorporation
1084 into glycogen (Two-way ANOVA, ∅genotype $p$=0.0372, $F$(1,24)=4.864); (E) $^{14}$C-glucose
1085 incorporation into lipid (Two-way ANOVA, ^Insulin $p$=0.0009, F(1,21)=14.94); (F)
1086 Representative images of insulin signalling components; (G) pT308 Akt (Two-way ANOVA,
1087 ^Insulin $p$=0.0010, F(1,27)=13.75); (H) pS473 Akt (Two-way ANOVA, ^Insulin $p$<0.0001,
1088 F(1,28)=33.13), and; (I) pS642 TBC1D4 (Two-way ANOVA, ∅genotype $p$=0.0011,
1089 $F$(1,25)=13.60) in bilateral AAV6 HDAC4 and 5 mice administered insulin and isotopic
1090 glucose tracers. (J) Experimental overview of stable isotope metabolomics in the bilateral
1091 AAV6 HDAC4 and 5 overexpression model. (K) Total metabolite abundance (Paired t-test,
1092 #Lactate $p$=0.0447, #Succinate $p$=0.0230); (L) Total $^{13}$C labelling of glycolytic and TCA cycle
1093 metabolites (Paired t-test, #Succinate $p$<0.0001, #Malate $p$=0.0337); (M) Lactate
1094 isotopologue (Paired t-test, #M0 $p$=0.0448, #M2 $p$=0.0299); (N) Succinate isotopologues
1095 (Paired t-test, #M0 $p$=0.0230, #M1 $p$=0.0002, #M2 $p$=0.0005), and; (O) Malate isotopologues
1096 (Paired t-test, #M1 $p$=0.0178) in bilateral AAV6 HDAC4 and 5 mice administered $^{13}$C- glucose
1097 tracer. (E) Data are mean±SEM, n=5-8 per group.
1098
1099 **Figure 3 - source data 1:** Source data for Figure 3B
1100
1101 **Figure 3 - source data 2:** Source data for Figure 3C
1102
1103 **Figure 3 - source data 3:** Source data for Figure 3D
1104
1105 **Figure 3 - source data 4:** Source data for Figure 3E
1106
1107 **Figure 3 - source data 5:** Raw blots for Figure 3F
1108
1109 **Figure 3 - source data 6:** Source data for Figure 3G
1110
1111 **Figure 3 - source data 7:** Source data for Figure 3H
1112
1113 **Figure 3 - source data 8:** Source data for Figure 3I
1114
1115 **Figure 3 - source data 9:** Source data for Figure 3K
1116
1117 **Figure 3 - source data 10:** Source data and raw blots for Figure 3L
1118
1119 **Figure 3 - source data 11:** Source data for Figure 3M
1120
1121 **Figure 3 - source data 12:** Source data for Figure 3N
1122
1123 **Figure 3 - source data 13:** Source data and raw blots for Figure 3O
1124
1125
1126 **Figure 3 Supplement** – Plasma tracer and muscle glycogen concentrations.
1127
1128 **Figure 3 supplement – source data 1:** Source data for Figure S3A
1129

**Figure 3 supplement – source data 2:** Source data for Figure S3B

**Figure 3 supplement – source data 3:** Source data for Figure S3C

**FIGURE 4**

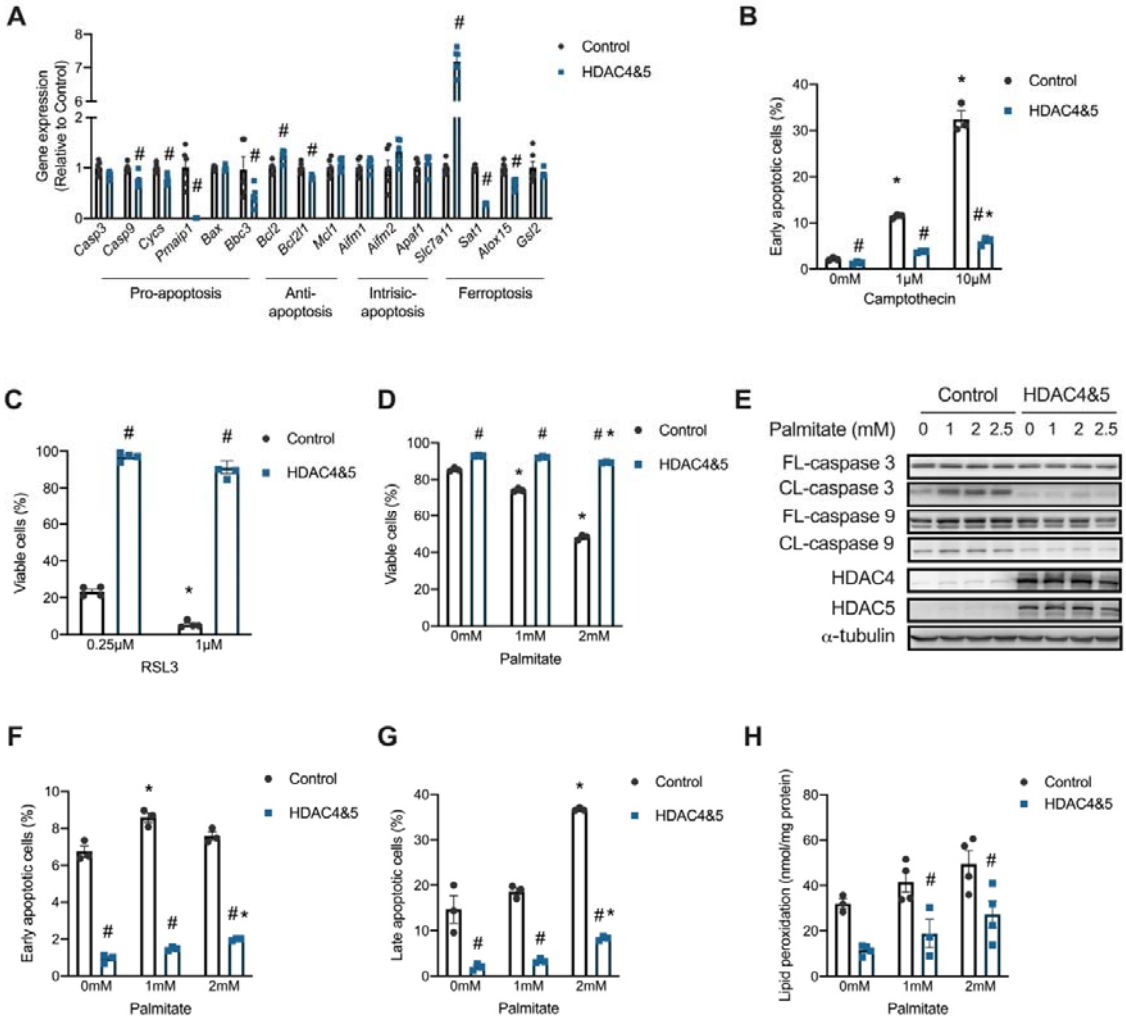


**Figure 4: HDAC and 5 enhance cell survival in response to lipotoxicity and supress the apoptosis and ferroptosis cell death pathways.** (A) Expression of p53-dependent genes involved in pro-apoptosis, anti-apoptosis, intrinsic apoptosis and ferroptosis (Unpaired t-test, #*Casp9* $p$=0.0258, #*Cycs* $p$=0.0049, #*Pmaip1* $p$=0.0010, #*Bbc3* $p$=0.0476, #*Bcl2* $p$=0.0037, #*Bcl2l1* $p$=0.0005, #*Slc7a11* $p$<0.0001, #*Sat1* $p$<0.0001, #*Alox15* $p$=0.0041); (B) Early apoptotic cells in response to the apoptosis-inducing agent Camptothecin (Two-way ANOVA, genotype $p$<0.0001 $F(1,12)$=349.3, treatment $p$<0.0001 $F(2,12)$=270.4, interaction $p$<0.0001 $F(2,12)$=149.5; #p<0.05 vs Control for same treatment, *p<0.05 vs vehicle by Tukey's multiple comparisons tests); (C) Cell viability in response to the ferroptosis-inducing agent RSL3 (Two-way ANOVA, genotype $p$<0.0001 $F(1,12)$=1645, treatment $p$<0.0001 $F(1,12)$=36.09, interaction $p$<0.0090 $F(1,12)$=9.665; #p<0.05 vs Control for same treatment, *p<0.05 vs 0.25μM RSL by Tukey's multiple comparisons tests); (D) Cell viability in response to palmitate (Two-way ANOVA, genotype $p$<0.0001 $F(1,12)$=3374, treatment $p$<0.0001 $F(2,12)$=1012, interaction $p$<0.0001 $F(2,12)$=684.8; #p<0.05 vs Control for same treatment, *p<0.05 vs vehicle by Tukey's multiple comparisons tests); (E) Full-length (FL) and cleaved (CL) caspase 3 and 9 in response to palmitate; (F) Early apoptotic cells in response to

palmitate (Two-way ANOVA, genotype $p<0.0001$ $F(1,12)=1468$, treatment $p=0.0001$ $F(2,12)=20.35$, interaction $p<0.0050$ $F(2,12)=8.498$; $^{\#}p<0.05$ vs Control for same treatment, $^{*}p<0.05$ vs vehicle by Tukey's multiple comparisons tests); (G) Late apoptotic cells in response to palmitate (Two-way ANOVA, genotype $p<0.0001$ $F(1,12)=313.4$, treatment $p<0.0001$ $F(2,12)=67.31$, interaction $p=0.0001$ $F(2,12)=21.00$; $^{\#}p<0.05$ vs Control for same treatment, $^{*}p<0.05$ vs vehicle by Tukey's multiple comparisons tests), and (H) Lipid peroxidation in response to palmitate (Two-way ANOVA, genotype $p<0.0001$ $F(1,12)=313.4$, treatment $p<0.0103$ $F(2,12)=67.31$; $^{\#}p<0.05$ vs Control for same treatment by Tukey's multiple comparisons tests) in Control and HDAC4 and 5 overexpressing C2C12 myoblasts. Data are mean±SEM, n=3-4 biological replicates per group.

**Figure 4 - source data 1:** Source data for Figure 4A

**Figure 4 - source data 2:** Source data for Figure 4B

**Figure 4 - source data 3:** Source data for Figure 4C

**Figure 4 - source data 4:** Source data for Figure 4D

**Figure 4 - source data 5:** Raw blots for Figure 4E

**Figure 4 - source data 6:** Source data for Figure 4F

**Figure 4 - source data 7:** Source data for Figure 4G

**Figure 4 - source data 8:** Source data for Figure 4H

**Figure 4 Supplement** - Characterisation of HDAC4&5 overexpression in C2C12 myoblasts.

**Figure 4 supplement – source data 1:** Raw blots for Figure S4A

**Figure 4 supplement – source data 2:** Source data for Figure S4B

**Figure 4 supplement – source data 3:** Source data for Figure S4C

**Figure 4 supplement – source data 4:** Source data for Figure S4D

**FIGURE 5**

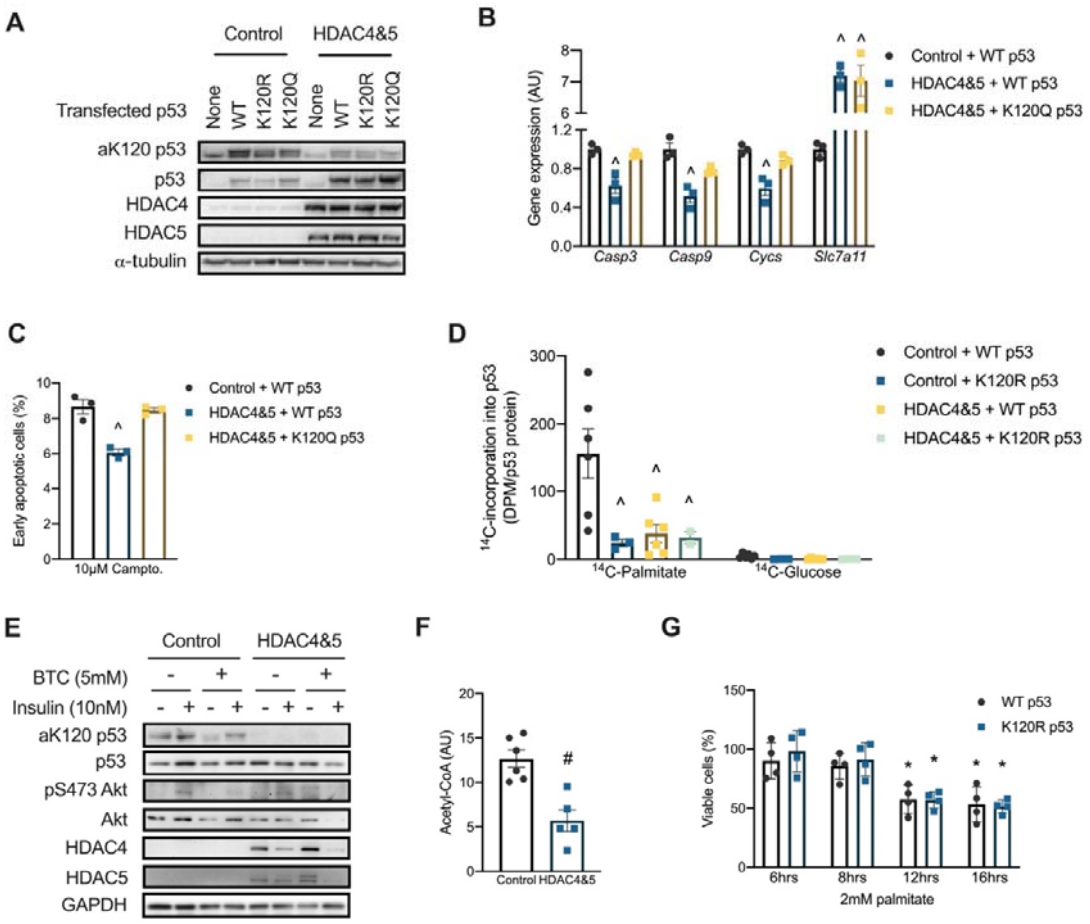


**Figure 5: HDAC4 and 5 suppress apoptosis by reducing p53 K120 acetylation, which is regulated by HDAC4 and 5-mediated alterations in metabolism.** (A) Acetylated p53 at lysine 120 (aK120 p53); (B) Expression of caspase 3 (*Casp3;* One-way ANOVA $p$=0.0040 $X^2$=0.8408, ^$p$<0.05 vs Control + WT p53 and HDAC4&5 + K120Q p53 by Tukey's multiple comparisons test), caspase 9 (*Casp9;* One-way ANOVA $p$=0.0025 $X^2$=0.8650, ^$p$<0.05 vs Control + WT p53 and HDAC4&5 + K120Q p53 by Tukey's multiple comparisons test), cytochrome c (*Cycs;* One-way ANOVA $p$=0.0033 $X^2$=0.8518, ^$p$<0.05 vs Control + WT p53 by Tukey's multiple comparisons test) and the cystine/glutamate antiporter xCT (*Slc7a11;* One-way ANOVA $p$<0.0001 $X^2$=0.9769, ^$p$<0.05 vs Control + WT p53 by Tukey's multiple comparisons test); (C) Percentage of early apoptotic cells following exposure to camptothecin (One-way ANOVA $p$=0.0008 $X^2$=0.9065, ^$p$<0.05 vs Control + WT p53 and HDAC4&5 + K120Q p53 by Tukey's multiple comparisons test); (D) $^{14}$C incorporation into p53 from palmitate (One-way ANOVA, $p$=0.0115 $X^2$=0.5602, ^p<0.05 vs Control + WT p53 by Tukey's multiple comparisons tests) or glucose; (E) aK120 p53 following expose to vehicle or insulin for 15 min following 24 hrs in the presence or absence of BTC; (F) Acetyl-CoA levels (Unpaired t-test, $p$=0.0014), and; (G) Cell viability 6, 8, 12 and 16 hrs after palmitate exposure (Two-way ANOVA, time $p$=0.0003 $F(1,6)$=52.34; $^*$p<0.05 vs 6hrs and 8hrs for same genotype by Tukey's multiple comparisons tests) in Control or HDAC4 and 5 overexpressing C2C12 myoblasts also expressing wild type (WT), K120R (loss-of-function) and K120Q (gain-of-function) p53. Data are mean±SEM, n=3-6 biological replicates per group.

1219 **Figure 5 - source data 1:** Raw blots for Figure 5A
1220
1221 **Figure 5 - source data 2:** Source data for Figure 5B
1222
1223 **Figure 5 - source data 3:** Source data for Figure 5C
1224
1225 **Figure 5 - source data 4:** Source data for Figure 5D
1226
1227 **Figure 5 - source data 5:** Raw blots for Figure 5E
1228
1229 **Figure 5 - source data 6:** Source data for Figure 5F
1230
1231 **Figure 5 - source data 7:** Source data for Figure 5G
1232
1233
1234
1235 **Figure 5 Supplement** – Bioenergetics in response to wild type and mutant p53
1236 overexpression.
1237
1238 **Figure 5 supplement – source data 1:** Source data for Figure S5A
1239
1240 **Figure 5 supplement – source data 2:** Source data for Figure S5B
1241

**FIGURE 6**

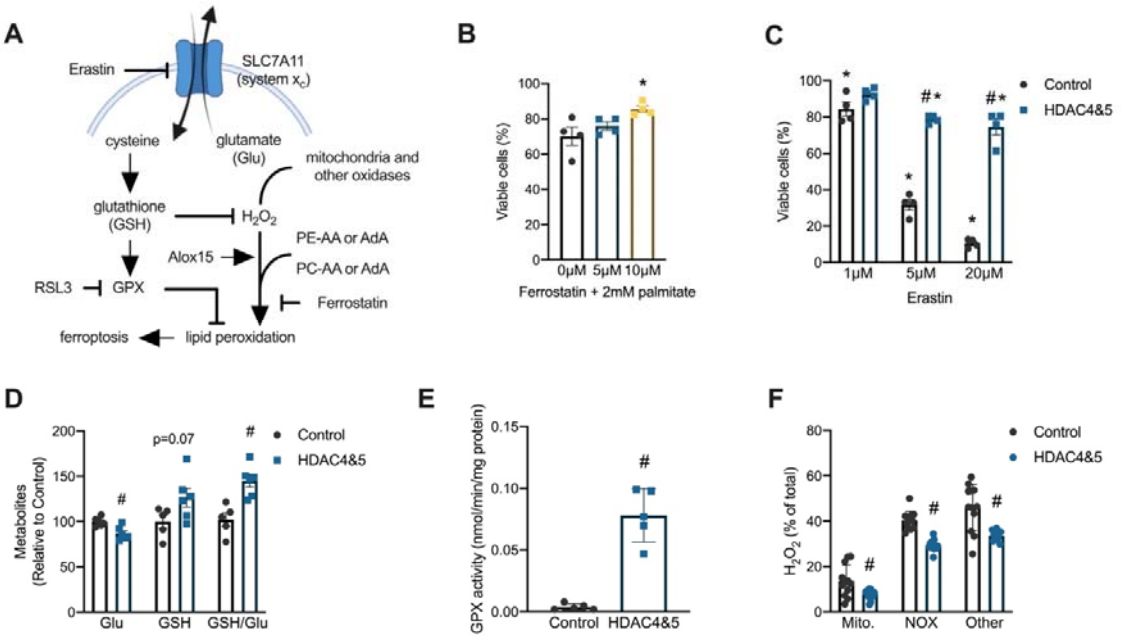


**Figure 6: HDAC4 and 5 regulate multiple metabolic inputs to the ferroptosis pathway.** (A) Schematic showing key regulatory points in the ferroptosis pathway. (B) Cell viability following palmitate exposure and co-incubation with vehicle (DMSO) or increasing concentrations of Ferrostatin (One-way ANOVA $p$=0.0323 $X^2$=0.5337, *$p$<0.05 vs Vehicle by Tukey's multiple comparisons test); (C) Cell viability following exposure to increasing concentrations of Erastin (Two-way ANOVA, genotype $p$<0.0001 $F$(1,18)=293.7, treatment $p$<0.0001 $F$(2,18)=139.6, interaction $p$<0.0001 $F$(2,18)=50.88; #p<0.05 vs Control for same treatment, *p<0.05 vs Vehicle same genotype by Tukey's multiple comparisons tests); (D) Glutamate (Glu), glutathione (GSH) and the GSH/Glu ratio (Unpaired t-tests, #Glu $p$=0.0049, #GSH/Glu $p$=0.0023); (E) Glutathione peroxidase (GPX) activity (Unpaired t-test, $p$<0.0001), and; (F) $H_2O_2$ derived from mitochondria (mito), NADPH oxidases (NOX) and other sources (Unpaired t-tests, #Mito $p$=0.0105, #NAPDH Ox. $p$<0.0001, #Other $p$=0.0004) in Control or HDAC4 and 5 overexpressing C2C12 myoblasts. Data are mean±SEM, n=4-10 biological replicates per group.

**Figure 6 - source data 1:** Source data for Figure 6B

**Figure 6 - source data 2:** Source data for Figure 6C

**Figure 6 - source data 3:** Source data for Figure 6D

**Figure 6 - source data 4:** Source data for Figure 6E

**Figure 6 - source data 5:** Source data for Figure 6F

1272
1273 **Figure 6 Supplement** – ROS and phospholipid responses to HDAC4&5 overexpression.
1274
1275 **Figure 6 supplement – source data 1:** Source data for Figure S6A
1276
1277 **Figure 6 supplement – source data 2:** Source data for Figure S6B
1278
1279 **Figure 6 supplement – source data 3:** Source data for Figure S6C
1280
1281 **Figure 6 supplement – source data 4:** Source data for Figure S6D
1282

1283
1284 **FIGURE 7**
1285

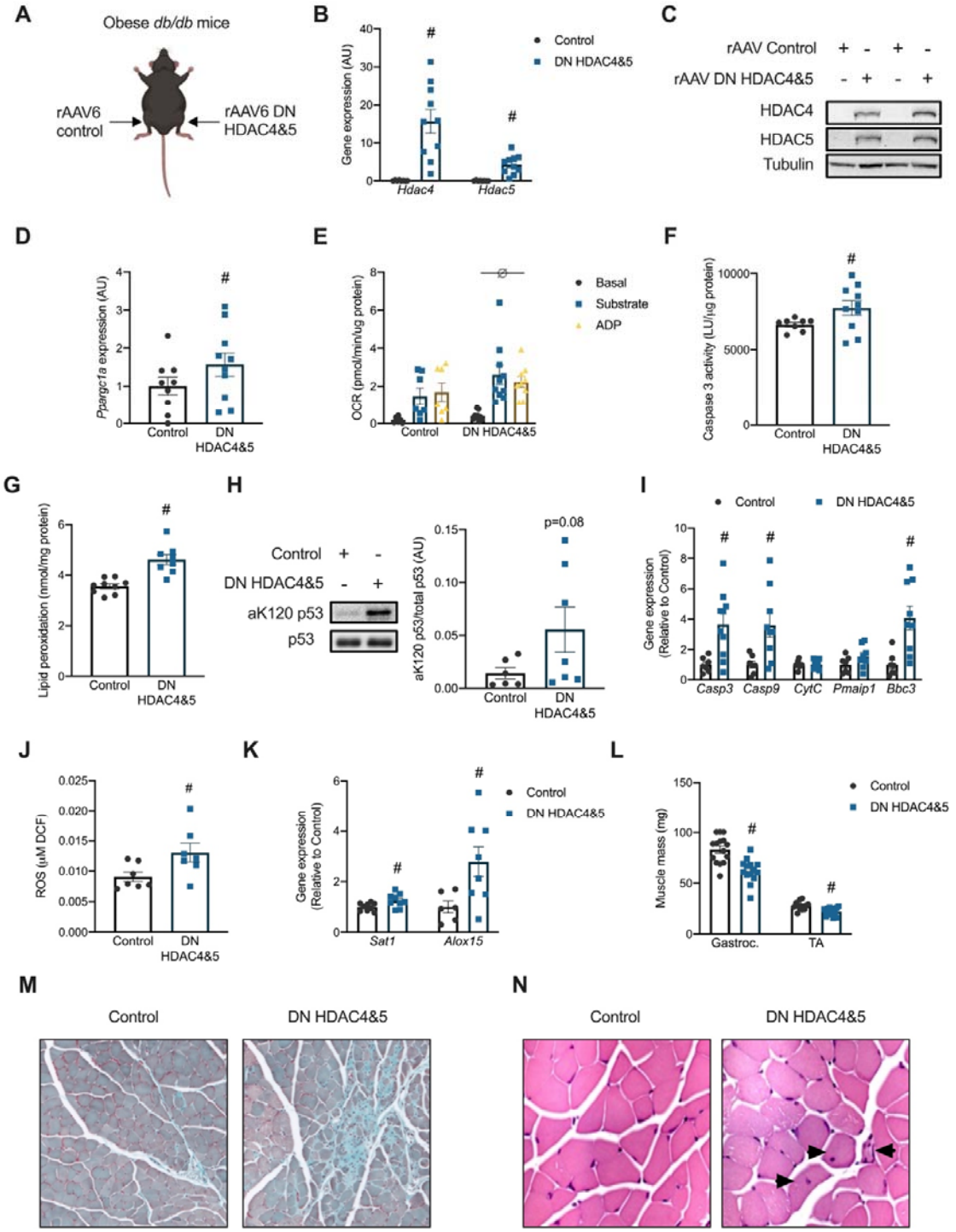


1286
1287

1288 **Figure 7: HDAC4 and 5 are required to suppress apoptosis and ferroptosis and maintain**
1289 **muscle mass in obese mice.** (A) The bilateral AAV6 dominant negative (DN) HDAC4 and 5
1290 overexpression *db/db* mouse model. (B) *Hdac4* and *Hdac5* gene expression (Paired t-tests,
1291 #*Hdac4* $p$=0.0004, #*Hdac5* $p$=0.0002); (C) HDAC4 and 5 protein; (D) *Ppargc1a* gene

expression (Paired t-tests, $p$=0.0191); (E) Basal, substrate and ADP-driven oxygen consumption rate (OCR) from muscle biopsies (Two-way ANOVA, genotype $p$=0.0482 $F(1,42)$=4.141); (F) Caspase 3 activity (Paired t-tests, $p$=0.0292); (G) Lipid peroxidation (Paired t-tests, $p$=0.0013); (H) Acetylated p53 at lysine 120 (aK120 p53); (I) Expression of apoptosis genes (Paired t-tests, #*Casp3* $p$=0.0072, #*Casp9* $p$=0.0129, #*Bbc3* $p$=0.0049); (J) Reactive oxygen species (ROS; Paired t-tests, $p$=0.0399); (K) Expression of ferroptosis genes (Paired t-tests, #*Sat1* $p$=0.0258, #*Casp9* $p$=0.0286); (L) Mass of the gastrocnemius (Gastroc.) and tibialis anterior (TA) skeletal muscles (Paired t-tests, #Gastroc. $P$<0.0001, #TA $p$=0.0004); (M) Masson's trichrome staining, and; (N) H&E staining of sections of the TA muscle in Control and DN HDAC4 and 5 overexpressing skeletal muscle in *db/db* mice. Arrows indicate fibres with centralised nuclei. Data are mean±SEM, n=6-10 per group.

**Figure 7 - source data 1:** Source data for Figure 7B

**Figure 7 - source data 2:** Raw blots for Figure 7C

**Figure 7 - source data 3:** Source data for Figure 7D

**Figure 7 - source data 4:** Source data for Figure 7E

**Figure 7 - source data 5:** Source data for Figure 7F

**Figure 7 - source data 6:** Source data for Figure 7G

**Figure 7 - source data 7:** Source data and raw blots for Figure 7H

**Figure 7 - source data 8:** Source data for Figure 7I

**Figure 7 - source data 9:** Source data for Figure 7J

**Figure 7 - source data 10:** Source data and raw blots for Figure 7K

**Figure 7 - source data 11:** Source data for Figure 7L

**Figure 7 Supplement** – *Slc7a11* expression, GPX activity and fibre diameter in response to DN HDAC4&5 expression in obese *db/db* mice.

**Figure 7 supplement – source data 1:** Source data for Figure S7A

**Figure 7 supplement – source data 2:** Source data for Figure S7B

**Figure 7 supplement – source data 3:** Source data for Figure S7C

1339 **FIGURE 8**

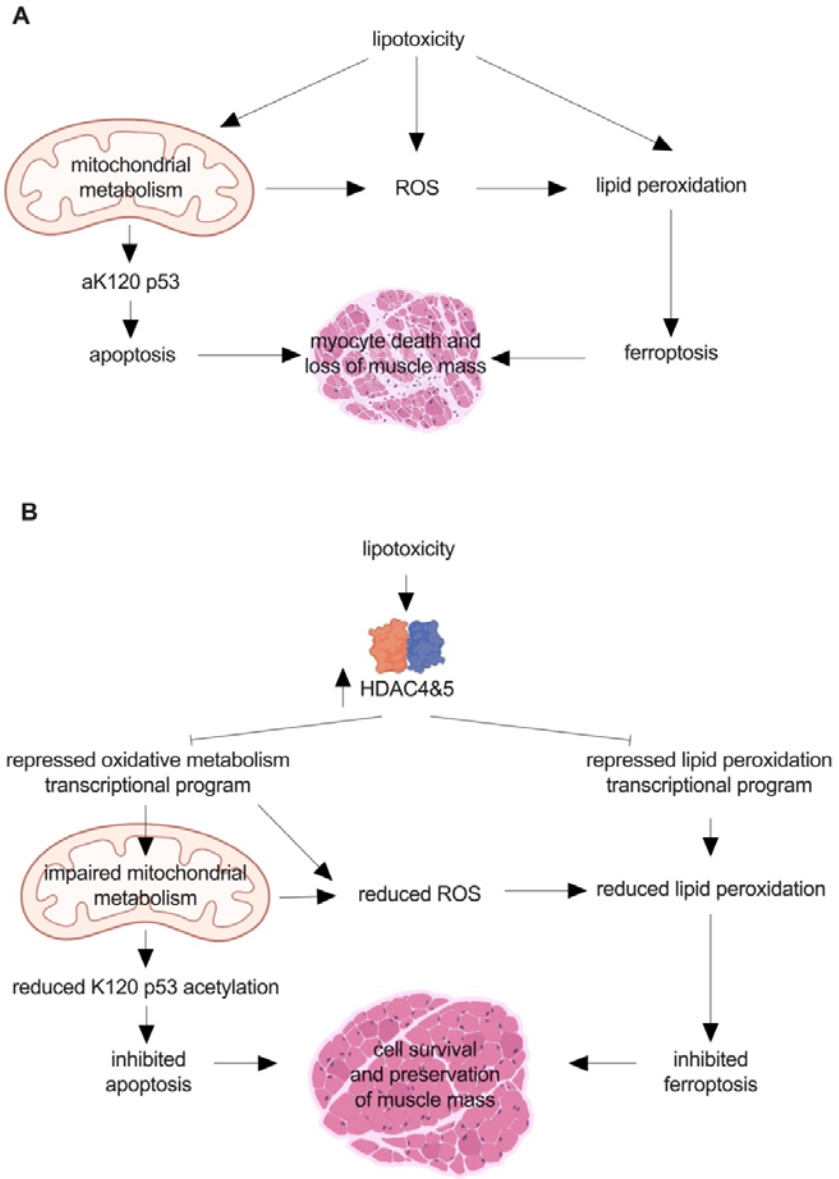


1340
1341
1342 **Figure 8: Proposed model.** (A) Lipotoxicity, through mitochondrial metabolism, increases
1343 acetylation of p53 and a transcriptional program that increases apoptosis. Lipotoxicity also
1344 increases reactive oxygen species (ROS) and lipid peroxidation, leading to ferroptosis.
1345 Activation of both apoptosis and ferroptosis increases myocyte death and loss of muscle
1346 mass. (B) Lipotoxicity increases HDAC4 and HDAC5, resulting in repression of a broad
1347 transcriptional program controlling oxidative metabolism and lipid peroxidation. Impaired
1348 mitochondrial metabolism reduces p53 acetylation at K120, which inhibits apoptosis.
1349 Similarly, p53-dependent genes involved in lipid peroxidation are reduced, which together
1350 with reduced ROS, inhibits lipid peroxidation and ferroptosis. Inhibition of both the
1351 apoptosis and ferroptosis cell death pathways preserves myocyte viability and muscle mass
1352 in response to lipotoxicity.
1353

**FIGURE SUPPLEMENT 1**

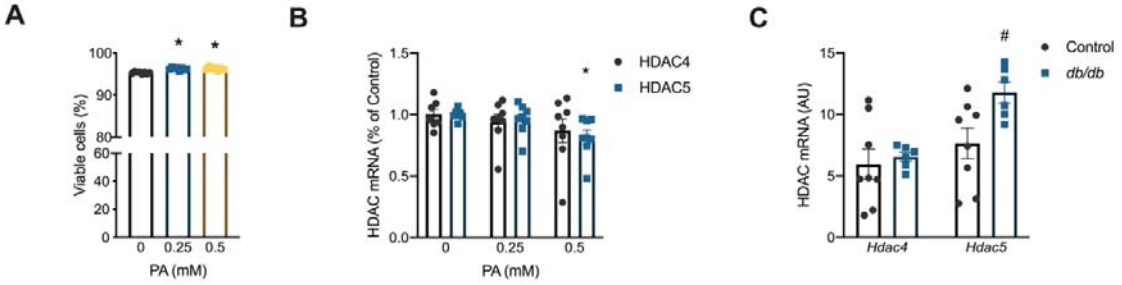


**Figure Supplement 1: Viability and gene expression responses to lipotoxicity.** (A) Viability of C2C12 myotubes (One-way ANOVA $p<0.0001$ $X^2=0.6927$, *$p<0.05$ vs Vehicle by Tukey's multiple comparisons test), and; (B) *Hdac4* and *Hdac5* gene expression following exposure to vehicle, 0.25mM or 0.5mM palmitate (PA) for 24hrs (One-way ANOVA $p=0.0195$ $X^2=0.3256$, *$p<0.05$ vs Vehicle by Tukey's multiple comparisons test). (C) *Hdac4* and *Hdac5* gene expression in tibialis anterior skeletal muscle from Control and *db/db* mice (Unpaired t-test, $p=0.0253$). Data are mean±SEM, n=6-8 biological replicates per group for cell experiments and 6-8 per group for animal experiments.

**FIGURE SUPPLEMENT 2**

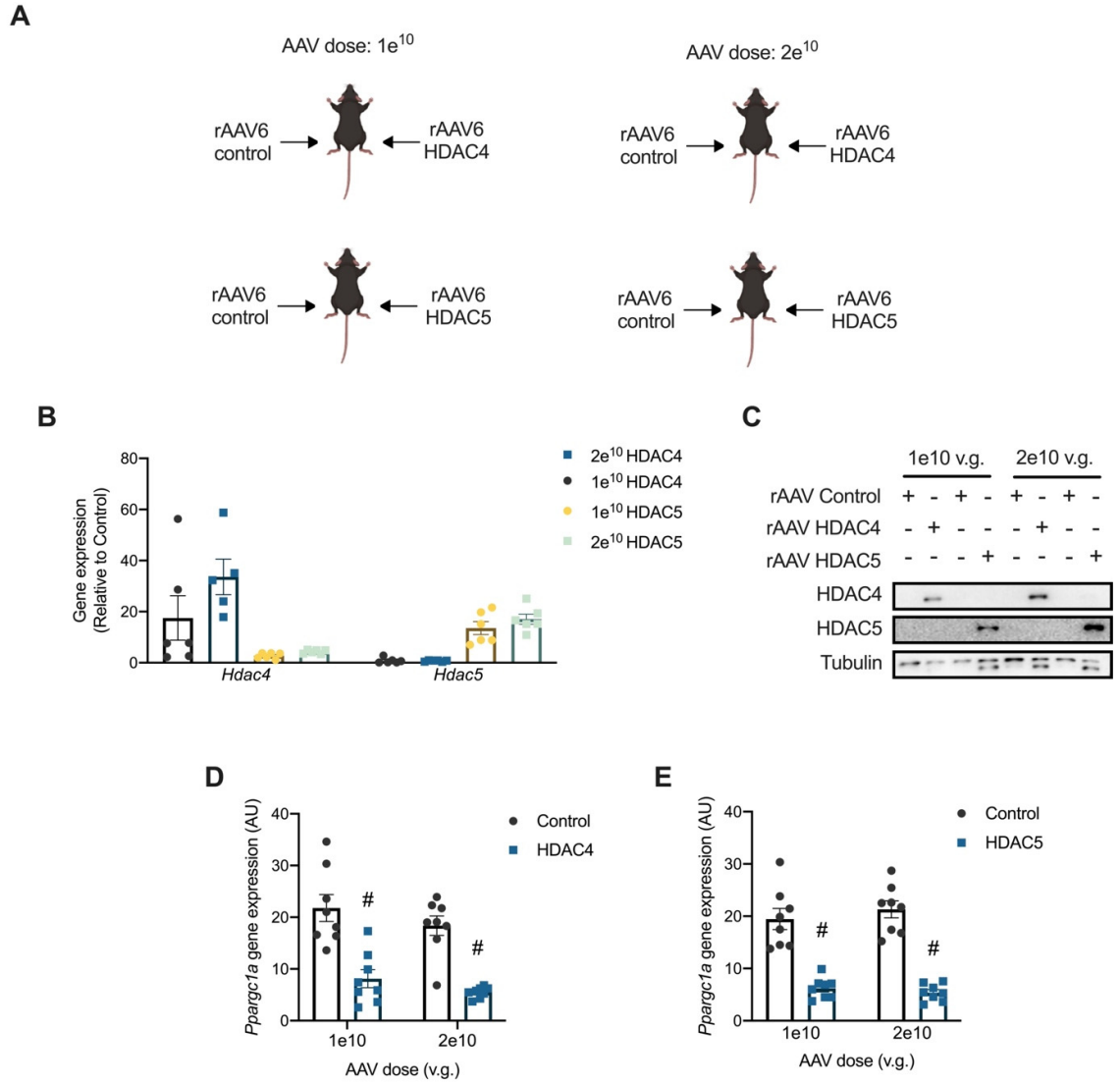


**Figure Supplement 2: Individual HDAC isoform and gene dosage effects on *Ppargc1a* expression.** (A) The bilateral AAV6 HDAC4 and 5 overexpression mouse model. (B) *Hdac4* and *Hdac5* gene expression; (C) HDAC4 and 5 protein; (D) and (E) *Ppargc1a* gene expression in skeletal muscle administered empty AAV6 (Control), HDAC4 AAV6 (Two-way ANOVA, genotype $p<0.0001$ $F(1,28)=52.30$; $^{\#}p<0.05$ vs Control for same AAV dose by Tukey's multiple comparisons tests) or HDAC5 AAV6 (Two-way ANOVA, genotype $p<0.0001$ $F(1,28)=112.7$; $^{\#}p<0.05$ vs Control for same AAV dose by Tukey's multiple comparisons tests). Data are mean±SEM, n=6-8 per group.

**FIGURE SUPPLEMENT 3**

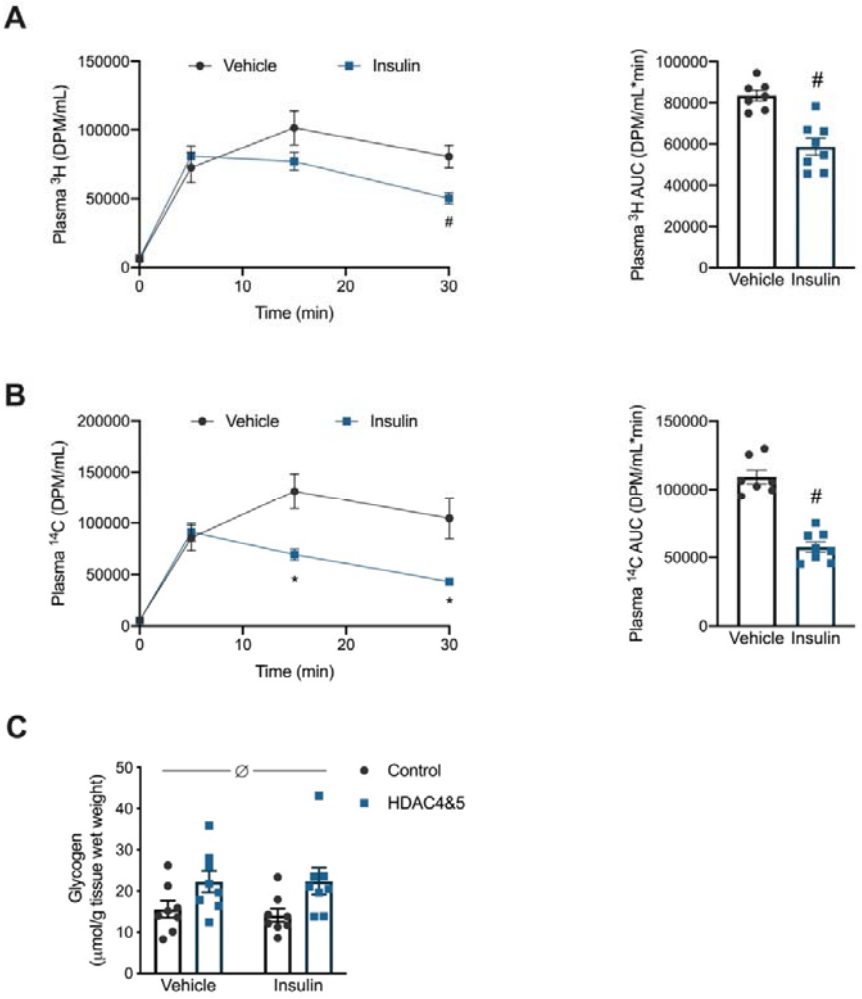


**Figure Supplement 3: Plasma tracer and muscle glycogen concentrations.** (A) Plasma $^{3}$H at 0, 5, 15 and 30 min (Two-way ANOVA, time $p<0.0001$ $F(2.607,36.5)=68.08$, interaction $p=0.0079$ $F(3,42)=4.511$, $^{\#}p<0.05$ vs Vehicle for same time point by Sidak's multiple comparisons tests) and plasma $^{3}$H area-under-the-curve (AUC; Unpaired t-test $p=0.0003$) following vehicle or insulin and $^{3}$H-2-deoxyglucose administration. (B) Plasma $^{14}$C at 0, 5, 15 and 30 min (Two-way ANOVA, time $p<0.0001$ $F(3,21)=47.84$, treatment $p=0.0442$ $F(1,7)=5.997$, interaction $p=0.0010$ $F(3,21)=7.944$, $^{\#}p<0.05$ vs Vehicle for same time point by Sidak's multiple comparisons tests) and plasma $^{14}$C AUC (Unpaired t-test $p<0.0001$) following vehicle or insulin and $^{14}$C-glucose administration. (C) Glycogen (Two-way ANOVA, $^{\varnothing}$genotype $p=0.0053$ $F(1,28)=9.131$) in Control or HDAC4 and 5 overexpressing skeletal muscle. Data are mean±SEM, n=6-8 per group.

**FIGURE SUPPLEMENT 4**

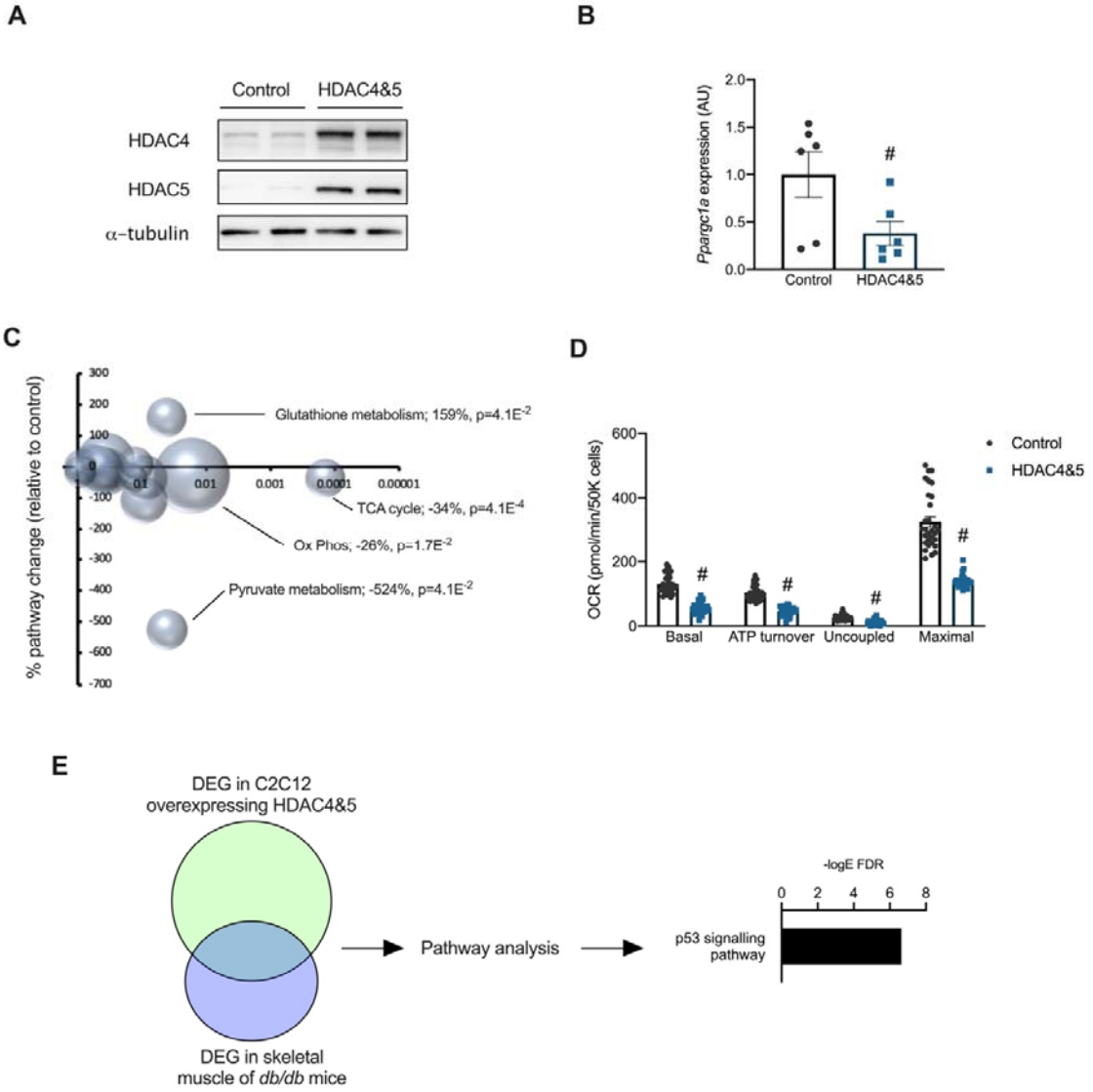


**Figure Supplement 4: Characterisation of HDAC4&5 overexpression in C2C12 myoblasts.** (A) HDAC4 and 5 protein; (B) *Ppargc1a* gene expression (Unpaired t-test, *p*=0.0475); (C) Bubble plot of metabolic pathway gene expression; (D) Oxygen consumption rate (OCR) linked to basal (Unpaired t-test, *p*<0.0001), ATP turnover (Unpaired t-test, *p*<0.0001), uncoupled (Unpaired t-test, *p*<0.0001) and maximal respiration (Unpaired t-test, *p*<0.0001) in Control and HDAC4 and 5 overexpressing C2C12 myoblasts. (E) Identification of co-differentially expressed genes in skeletal muscle from *db/db* mice and C2C12 myoblasts overexpressing HDAC4 and 5 (n=3/group for skeletal muscle and cell analyses) followed by pathway enrichment analysis revealed the p53 signalling pathway as being significantly enriched in this geneset. Data are mean±SEM, n=6-20 biological replicates per group. # p<0.05 vs Control.

**FIGURE SUPPLEMENT 5**

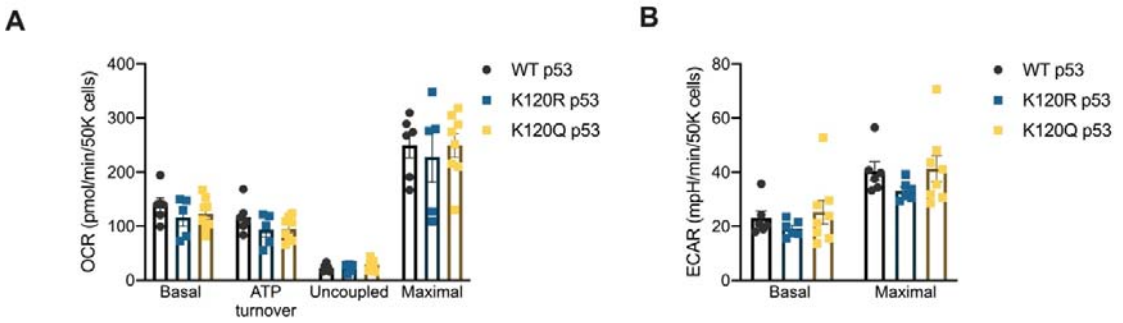


**Figure Supplement 5: Bioenergetics in response to wild type and mutant p53 overexpression.** (A) Oxygen consumption rate (OCR) linked to basal, ATP turnover, uncoupled and maximal respiration and (B) Basal and maximal extracellular acidification rate (ECAR) in C2C12 myoblasts expressing WT, K120R or K120Q p53. Data are mean±SEM, n=8 biological replicates per group.

**FIGURE SUPPLEMENT 6**

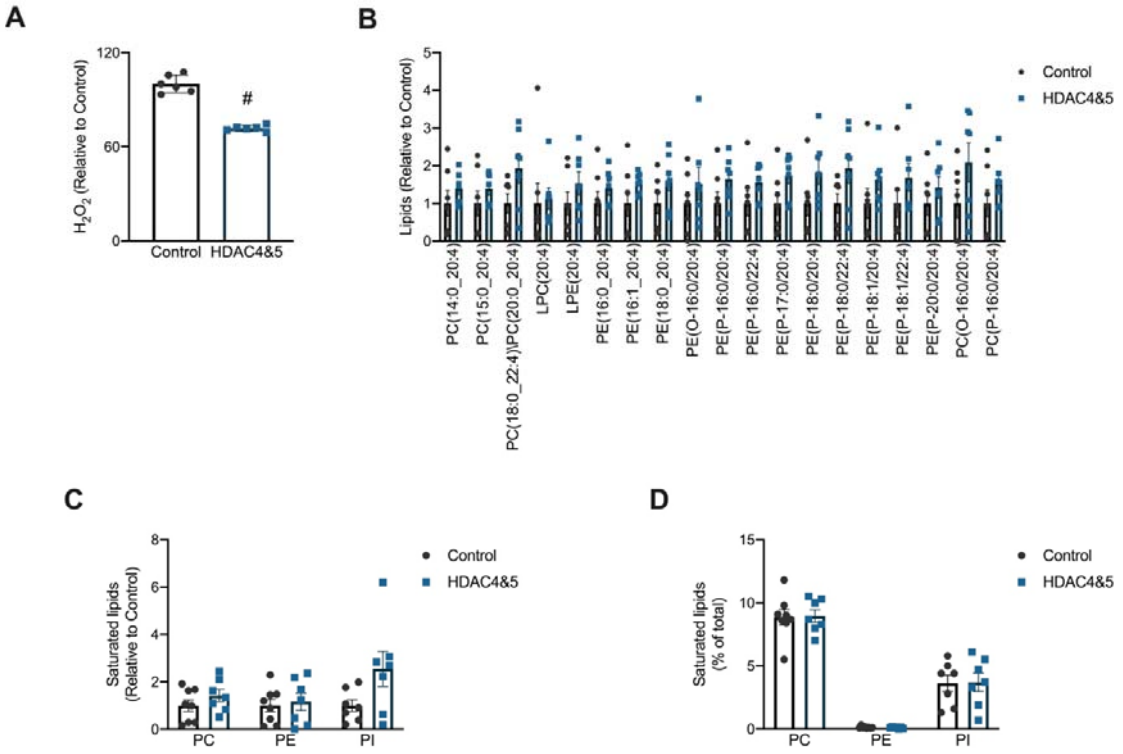


**Figure Supplement 6: ROS and phospholipid responses to HDAC4&5 overexpression.** (A) Total $H_2O_2$ release from Control and HDAC4 and 5 overexpressing C2C12 myoblasts (Unpaired t-test, $p<0.0001$). (B) Phosphatidylcholine (PC), lysophosphatidylcholine (LPC), lysophosphatidyl-ethanolamine (LPE) and phosphatidylethanolamine (PE) lipids; (C) Saturation of PC, PE and phosphatidylinositol (PI) lipids, and; (D) Saturation of PC, PE and PI lipids expressed as a percentage of total lipid within each species in Control or HDAC4 and 5 overexpressing skeletal muscle. Data are mean±SEM, n=6 biological replicates per group for cell experiments and n=7 per group in mouse experiments. # p<0.05 vs Control, ∅ p,0.05 main effect for genotype.

**FIGURE SUPPLEMENT 7**

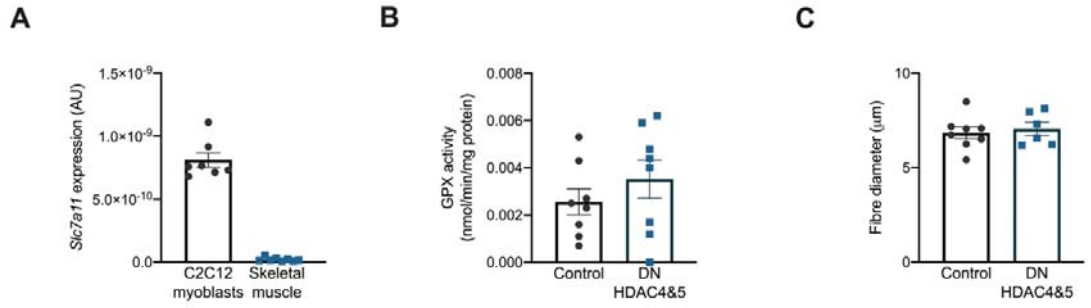


**Figure Supplement 7: *Slc7a11* expression, GPX activity and fibre diameter in response to DN HDAC4&5 expression in obese *db/db* mice.** (A) *Slc7a11* expression in C2C12 myoblasts or mouse skeletal muscle. (B) Glutathione peroxidase (GPX) activity, and; (C) Fibre diameter in Control and DN HDAC4 and 5 skeletal muscle of *db/db* mice. Data are mean±SEM, n=7-8 per group.